Intraflagellar Transport and Functional Analysis of Genes Required for Flagellum Formation in Trypanosomes.

Sabrina Absalon, Thierry Blisnick, Linda Kohl, Géraldine Toutirais, Gwénola Doré, Daria Julkowska, Arounie Tavenet, Philippe Bastin

Intraflagellar transport and functional analysis of genes required for flagellum formation in trypanosomes

Sabrina Absalon[1,2], Thierry Blisnick[1], Linda Kohl[2,3], Géraldine Toutirais[2], Gwénola Doré[2], Daria Julkowska[1], Arounie Tavenet[2] and Philippe Bastin[1,2]

[1] Trypanosome Cell Biology Unit, Pasteur Institute & CNRS, 25 rue du Docteur Roux, 75015 Paris, France

[2] Dynamique et Régulation des Génomes, Muséum National d'Histoire Naturelle, INSERM & CNRS, 43 rue Cuvier, 75005 Paris, France

[3]Biologie Fonctionnelle des Protozoaires, Muséum National d'Histoire Naturelle, 61 rue Buffon, 75005 Paris, France

Address correspondence to: Philippe Bastin (pbastin@pasteur.fr)

Abbreviations: IFA, immunofluorescence assay, IFT, intraflagellar transport; MAb, monoclonal antibody; PFA, paraformaldehyde; PFR, paraflagellar rod; PIFT, putatively involved in intraflagellar transport

Abstract

IntraFlagellar Transport (IFT) is the bidirectional movement of protein complexes required for cilia and flagella formation. We investigated IFT by analysing 9 conventional *IFT* genes and 5 novel Putative IFT genes (*PIFT*) in *Trypanosoma brucei*, that maintains its existing flagellum whilst assembling a new one. Immunostaining against IFT172 or expression of tagged IFT20 or GFP::IFT52 revealed the presence of IFT proteins along the axoneme and at the basal body and pro-basal body regions of both old and new flagella. IFT particles were detected by electron microscopy and exhibited a strict localisation to axonemal microtubules 3-4 and 7-8, suggesting the existence of specific IFT tracks. Rapid (> 3µm/sec) bidirectional intraflagellar movement of GFP::IFT52 was observed in old and new flagella. RNAi silencing demonstrated that all individual *IFT* and *PIFT* genes are essential for new flagellum construction but the old flagellum remained present. Inhibition of IFTB proteins completely blocked axoneme construction. Absence of IFTA proteins (IFT122, IFT140) led to formation of short flagella filled with IFT172, indicative of defects in retrograde transport. Two PIFT proteins turned out to be required for retrograde transport and 3 for anterograde transport. Finally, flagellum membrane elongation continues despite the absence of axonemal microtubules in all IFT/PIFT mutant.

Introduction

IntraFlagellar Transport (IFT) is the bi-directional movement of protein particles in the matrix of cilia and flagella, independent of flagellum beating (Kozminski *et al.*, 1993). IFT is driven by two microtubule-associated motor complexes: the heterotrimeric kinesin II that moves particles towards the tip (Kozminski *et al.*, 1995; Cole *et al.*, 1998; Snow *et al.*, 2004) and a dynein complex that displaces them from the tip to the base of the organelle (Pazour *et al.*, 1999; Porter *et al.*, 1999; Signor *et al.*, 1999). IFT particles have been purified by differential centrifugation from the matrix of isolated flagella from the green algae *Chlamydomonas.* They are composed of at least 17 proteins that can be separated into a complex A, made of 6 proteins, and a complex B that contains 11 proteins (Piperno and Mead, 1997; Cole *et al.*, 1998). These IFT proteins are rich in protein-protein interaction domains of the WD-40, TPR or coil-coiled families (Cole, 2003). Several of these proteins have been localised along the length of growing and mature cilia or flagella but a significant proportion is also found around the basal body area (Cole *et al.*, 1998; Deane *et al.*, 2001; Pedersen *et al.*, 2005).

IFT is required for the transport of flagellar precursors to the distal tip of the flagellum, the site of construction of the organelle (Qin *et al.*, 2004). Consequently, inhibition of IFT prevents flagellum assembly in most organisms studied so far (Kozminski *et al.*, 1995; Nonaka *et al.*, 1998; Brown *et al.*, 2003; Kohl *et al.*, 2003). The only exceptions are encountered in cell types that assemble their flagella in the cytoplasm, such as male gametes of *Drosophila* (Han *et al.*, 2003; Sarpal *et al.*, 2003) and of *Plasmodium* (Avidor-Reiss *et al.*, 2004; Briggs *et al.*, 2004a).

Analysis of *Chlamydomonas* and *C. elegans* IFT mutants indicates that complex B is associated to anterograde transport while complex A would be linked to retrograde transport

(Cole, 2003). Genetic, biochemical and morphological analysis from such mutants contributed to the understanding of the mode of action of IFT (Pedersen *et al.*, 2006; Ou *et al.*, 2007). Particles are assembled at the base of the flagellum and are moved towards the tip by kinesin II directly associated to complex B proteins (anterograde movement). Proteins from complex A, the inactive dynein motor complex and axonemal proteins are co-transported and unloaded at the distal end. Dynein becomes the active motor and associates to proteins of the A complex and travels back to the base of the flagellum where the cycle can re-initiate. Relatively few data are available about IFT regulation and the specific function of individual IFT proteins (Hou *et al.*, 2007). IFT is involved in both construction and maintenance of cilia and flagella but the differences between these two situations in the life of an organelle are poorly understood (Kozminski *et al.*, 1995).

Trypanosoma brucei is a flagellated protist responsible for sleeping sickness in central Africa. It is a fascinating organism to study as it exhibits a number of original features, including at the flagellar level (Kohl and Bastin, 2005). It possesses a single motile flagellum whose axoneme is assembled on a basal body flanked by an immature pro-basal body (Sherwin and Gull, 1989). The axoneme contains a central pair and peripheral doublets carry outer and inner dynein arms as well as radial spokes. Molecular components of these structures are conserved and functional analysis revealed their role in flagellum beating (Branche *et al.*, 2006; Broadhead *et al.*, 2006; Ralston *et al.*, 2006; Baron *et al.*, 2007). An extra-axonemal structure called the paraflagellar rod (PFR) is present alongside the axoneme from its point of emergence from the flagellar pocket until its distal tip (Bastin *et al.*, 1996). It is tightly linked to the axoneme *via* physical connections to microtubule doublets 4 to 7. This means that trypanosomes need to assemble separate structures during flagellum construction, a feature also encountered in spermatozoa (Escalier, 2003). PFR proteins are effectively transported towards the distal tip of the flagellum as demonstrated in mutants that

fail to assemble a full PFR structure (Bastin *et al.*, 1998; Bastin *et al.*, 1999b), although the actual motors are unknown. Like most protozoa, trypanosomes assemble a new flagellum at each cell cycle whilst conserving the old one (Sherwin and Gull, 1989), thereby providing the unique opportunity to compare mature and constructing flagella in the same cell. The presence of two flagella of different age and of different length raises the question as to how trypanosomes control IFT. We previously demonstrated that IFT88 (an IFT complex B protein also called Polaris or OSM-5) and the heavy chain dynein motor DHC1b were both required for flagellum formation in *T. brucei*, suggesting that IFT is functional in trypanosomes (Kohl *et al.*, 2003). Induction of RNAi silencing any of these two genes first leads to the production of shorter new flagella without affecting the existing old flagellum. Analysis of cells inheriting the shorter new flagellum revealed a surprising link with cell size suggesting that trypanosomes could control IFT to regulate flagellar length and subsequently cell size. Longer induction times completely blocked flagellum formation, producing short cells that rapidly lose polarity, exhibit defects in basal body positioning and fail to undergo cytokinesis (Kohl *et al.*, 2003; Absalon *et al.*, 2007). However, the existing old flagellum remains in place and appears intact. Some of these results have recently been reproduced upon silencing of the *IFT80* (*CHE-2*) gene that encodes another complex B protein (Davidge *et al.*, 2006).

Inducible expression of tagged flagellar proteins showed a strong bias towards the distal tip of the new flagellum with little incorporation in the mature flagellum (Bastin *et al.*, 1999a). To determine the role of IFT in this discrimination, we investigated IFT proteins, IFT particles and IFT movement in the old and the new flagella of *T. brucei*. We performed an extensive functional analysis of 9 genes known to be involved in IFT in other species and of 5 novel genes identified by comparative genomics as putatively involved in IFT (*PIFT* genes).

Materials and Methods

Trypanosome cell lines and cultures

All cell lines used for this work were derivatives of strain 427 of *T. brucei* and cultured in SDM79 medium supplemented with hemin and 10 % foetal calf serum. Cell lines *DHC1b*^{RNAi}, *IFT88*^{RNAi} (Kohl *et al.*, 2003), *IFT20*^{RNAi} (Absalon *et al.*, 2007), *PF16*^{RNAi} and *PF20*^{RNAi} (Branche *et al.*, 2006) have been described previously. They all express complementary single stranded RNA corresponding to a fragment of the gene of interest (300-900 bp) from two tetracycline-inducible T7 promoters facing each other in the pZJM vector (Wang *et al.*, 2000) transformed in 29-13 cells that express the T7 RNA polymerase and the tetracycline-repressor (Wirtz *et al.*, 1999). Addition of tetracycline to the medium induces expression of sense and antisense RNA strands that can anneal to form double-stranded RNA and trigger RNAi.

The *T. brucei* genome has been fully sequenced (Berriman *et al.*, 2005) and the GeneDB data base was searched for homologues of *Chlamydomonas* or *C. elegans IFT* genes. The list of genes studied here, their reference number in GeneDB and the name of homologues in the *C. elegans* and *D. melanogaster* genome data bases is given at Figure 1.

Plasmid construction and transformation in trypanosomes

For generation of cell lines expressing dsRNA for RNAi knock-down, sequences were selected according to their lack of significant identity with other genes to avoid cross-RNAi (Durand-Dubief *et al.*, 2003) using the RNAit algorithm (Redmond *et al.*, 2003). Primers are available on request from the authors. Gene fragments were amplified by PCR on *T. brucei* genomic DNA, purified on QIA-Quick columns (Qiagen), digested with *Hin*d III and *Xho* I and ligated in the corresponding sites of the pZJM vector.

For expression of IFT20 fused to a tap-tag, the whole *IFT20* sequence was amplified by PCR with the proof-reading enzyme *Pfu* I using GCGTGCCAAGCTTATGGATGATGATAAACTTGTG as forward primer (*Hin*d III site underlined) and GCATGATATCCTCACGCGAGGCGTGACTCAG (*Hpa* I site underlined) as reverse primer. The amplified product contains the complete coding sequence of IFT20 but the stop codon was not included. It was ligated in the *Hin*d III and *Eco* RV sites of the pHD918 (Estevez *et al.*, 2001) vector in such a way that the insertion of the *IFT20* coding sequence was in-frame with that coding for protein A, generating plasmid pIFT20TAPTAG918. For inducible expression of GFP::IFT52, the full coding sequence of *IFT52* was amplified by PCR using Phusion™ (Finnzyme) with GCATCATCTAGAATGACGGATGCCCCAAGG (*Xba* I site underlined) as forward primer and GCATCGGGATCCTCAAAGCTCCTCAATTTC as reverse primer (*Bam* HI site underlined), cloned in the pPCEGFPN2PFR vector (S.A. et al, unpublished data) and the fusion gene encoding GFP::IFT52 was transferred to the pHD430 inducible expression vector (Wirtz and Clayton, 1995). All inserted sequences and flanking regions were sequenced to confirm correct integration and fusion (Genome Express).

For transfection, pZJM plasmids were linearised with *Not* I and individually transformed in 29-13 cells. pIFT20TAPTAG918 and pGFPIFT52430 were transformed in the rDNA locus of the PTP or PTH cell lines that express the tet-repressor from the pHD449 or the pHD360 vectors, respectively (Wirtz and Clayton, 1995; Bastin *et al.*, 1999a). In all cases, transfected cells were immediately cloned and all antibiotic-resistant cell lines were characterised by immunofluorescence with the anti-PFR2 antibody L8C4 or with the anti-protein A antibody (Sigma) or by direct fluorescence observation (GFP). Clones with the clearest distinction between non-induced and induced samples were selected for sub-cloning

by limiting dilution. RNAi was induced by addition of 1 µg tetracycline per ml of medium and fresh tetracycline was added at each cell dilution.

Protein expression and antibody production

Given the large size of IFT172, only a fragment was cloned and expressed in *E. coli*. The forward primer GATGAACGGATCCGCTATTCAAGCATACAAAAAGG was used (*Bam* HI site underlined) and CCGTGCGAATTCGCTACACGAACAGCATCCTCC served as reverse primer (*Eco* RI site underlined), representing nucleotides 2500-3270 of the *IFT172* coding sequence. The PCR product was amplified using a proof-reading enzyme, digested with *Bam* HI and *Eco* RI and ligated in compatible sites of the pGEXB vector for protein expression. The plasmids were sequenced to confirm identity and correct fusion with GST. Plasmids were transformed in the competent BL21 strain of *E. coli* and protein expression was analysed by SDS-PAGE followed by Coomassie staining. GST coupled proteins were purified as described (Smith and Johnson, 1988) and 20 µg were injected to BALB/C mice for immunisation. After bleeding, sera were absorbed against GST. Sera from mice immunised with GST alone were used as negative controls.

Immunofluorescence and light microscopy analysis

For immunofluorescence with the anti-IFT172 antiserum, intact cells or detergent-extracted cytoskeletons (see below) were washed, settled on poly-L-lysine coated slides and fixed either in 4 % paraformaldehyde (PFA) for 10 minutes or in methanol for at maximum of 5 minutes at -20°C. In the case of PFA fixation, cells were permeabilised with 0.1 % Nonidet P-40 for 10 minutes and samples were rinsed to remove the excess of detergent. Blocking was performed by an incubation of 45-60 minutes in PBS containing 0.1 % bovine serum albumin

and washed slides were incubated with 1:200 dilution of antiserum for 45-60 minutes. Slides were washed and incubated with anti-mouse secondary antibodies coupled to Alexa 488 (Invitrogen). For detergent treatment, cells were settled on poly-L-lysine coated slides and exposed to 1 % Nonidet P-40 in PEM buffer (100 mM Pipes (pH 6.9), $MgCl_2$ 1 mM and EGTA 1 mM). For cells expressing the IFT20::TAP tag, both PFA and methanol fixations were used, with a dilution of 1:10,000 of the anti-protein A antibody (Sigma). For cytoskeletons of GFP::IFT52 expressing cells, samples were settled on slides and briefly exposed to 1 % Nonidet P-40 in 4 M glycerol, 10 mM PIPES (pH 6.5), 10 mM $MgCl_2$ and 5 mM EGTA, washed and processed as above. The monoclonal antibody L8C4 (IgG1), that specifically recognises PFR2 was used as marker of flagellum assembly (Kohl *et al.*, 1999). The monoclonal antibody MAb22 is an IgM that detects an as yet unidentified antigen found at the proximal zone of both the mature and the pro-basal body (M. Bonhivers and D. Robinson, unpublished data)(Pradel *et al.*, 2006). MAb25 is an IgG2a that recognises a protein found all along the axoneme (M. Bonhivers and D. Robinson, unpublished data)(Pradel *et al.*, 2006). The MAb 20H5 recognises centrins and was used at a 1:400 dilution (Sanders and Salisbury, 1994). A rabbit antiserum raised against the *Leishmania donovani* centrin 1 was used at a 1:1,000 dilution (Selvapandiyan *et al.*, 2007). GFP was observed directly or upon immunofluorescence using an anti-GFP antibody (Invitrogen). Sub-class specific secondary antibodies coupled to FITC (Sigma), Alexa 488 or Alexa 594 (Invitrogen), Cy3 or Cy5 (Jackson) were used for double labelling. Slides were stained with DAPI for visualisation of kinetoplast and nuclear DNA content. For visualisation of GFP on live cells, trypanosomes cultures were mixed with a solution of 3 % LMP agarose (BioRad) to reduce cell movement. Samples were observed with a DMR Leica microscope and images were captured with a Cool Snap HQ camera (Roper Scientific). Alternatively, slides were also viewed on a DMI4000 Leica microscope and images were acquired with a Retiga-SRV

camera (Q-Imaging). Images were analysed and cell parameters were measured using the IPLab Spectrum 3.9 software (Scanalytics & BD Biosciences) or Image J. For movies, cells were filmed using a Cohu camera 460LI and images were recorded using a DVD recorder.

Electron microscopy

Cell fixation, embedding and sectioning for transmission electron microscopy of whole cells or of detergent-treated samples was carried out as described previously (Branche *et al.*, 2006). For scanning electron microscopy, cells were washed in PBS, fixed with 2.5 % glutaraldehyde and treated as reported previously (Absalon *et al.*, 2007).

RT-PCR

Total RNA was extracted from cells grown with or without tetracycline for the indicated periods of time and purified using Trizol. DNA was eliminated by DNase treatment and RNA purity was confirmed by conventional PCR. After primer calibration and determination of optimal conditions, semi-quantitative RT-PCR was performed as described (Durand-Dubief *et al.*, 2003). At least one primer was selected to be outside the region selected for dsRNA expression to avoid amplification of RNA deriving from the dsRNA trigger.

Western blot

Cells were washed in PBS, homogenised and boiled in gel sample buffer before SDS-PAGE. Proteins were transferred to PVDF membranes and incubated with the anti-protein A antibody (1:1,000) or with the anti-GFP antibody (1:800). Membranes were probed with the anti-PFR antibody L13D6 (dilution 1:50), or with a rabbit anti-aldolase (dilution 1:1,000) antibody as loading control and revealed with ECL+ (Amersham).

Results

Identification of IFT-related genes in trypanosomes

To identify trypanosome genes participating in flagellum formation, we first searched the *T. brucei* genome for genes encoding proteins known to be components of purified IFT particles in *Chlamydomonas* (Cole *et al.*, 1998). At the time this study was initiated, the sequences of 8 genes encoding IFT proteins were available: *IFT122, IFT140* (complex A) and *IFT20, IFT52, IFT57/55*, *IFT80, IFT88, IFT172* (complex B) (*C. elegans* and *D. melanogaster* gene nomenclature is given at Figure 1). The corresponding trypanosome genes are all present in the *T. brucei* genome data base (Kohl *et al.*, 2003; Briggs *et al.*, 2004a; Berriman *et al.*, 2005; Absalon *et al.*, 2007) and exhibit 21-55 % overall identity with orthologues from various species (Figure 1), a value in the same range as what was found for axonemal proteins (Branche *et al.*, 2006; Ralston *et al.*, 2006; Baron *et al.*, 2007). In addition, the gene encoding the IFT dynein heavy chain previously identified and functionally characterised in our laboratory was also included in this study, hence providing a total of 9 IFT-related genes.

Next, we searched to identify novel genes encoding proteins possibly involved in the IFT process but that were not purified with IFT particles. As the only flagella of *Plasmodium* are found in the male gametes and are assembled in the cytoplasm, *IFT* genes are absent from the genome of this group of species. By contrast, genes encoding proteins of the dynein arms or central pair components of the axoneme are conserved (Avidor-Reiss *et al.*, 2004; Kohl and Bastin, 2005). This provides the opportunity to compare the genomes of *Plasmodium* spp with these of other ciliated species and to discriminate genes encoding proteins involved in IFT from genes encoding structural components of the flagellum. A similar approach was successfully employed to identify genes encoding flagellar proteins involved in beating by

comparison of species with motile or non-motile flagella (Baron *et al.*, 2007). Comparison of genomes from species assembling their flagella with or without IFT indicated that at least 27 genes are conserved in species assembling their flagella by IFT (Avidor-Reiss *et al.*, 2004). We selected 5 of these genes that are conserved in *T. brucei* for functional analysis and termed them *PIFT* for Putative IntraFlagellar Transport genes (Figure 1). The PIFTA1 protein presents coiled-coil domains whereas the PIFTB2 and PIFTC3 protein contain TPR domains, a feature shared with IFT88 and IFT139 (Cole, 2003). PIFTD4 and PIFTF6 both contain two WD-40 domains at their amino terminal region and a TPR motif towards the centre of their sequence. PIFTE5 exhibits a different structure and will be reported elsewhere. The five trypanosome *PIFT* genes are the homologues of the recently identified *DYF-3*, *DYF-1*, *DYF-13, IFTA-1* and *DYF-2* respectively, known to be linked to the formation of sensory cilia in *C. elegans* (Starich *et al.*, 1995; Blacque *et al.*, 2005; Murayama *et al.*, 2005; Bell *et al.*, 2006; Blacque *et al.*, 2006; Efimenko *et al.*, 2006). PIFTD4 and PIFTF6 are the homologues of the OSEG4 and OSEG6 proteins that localise to the Outer SEGment of sensory cilia in *Drosophila* (Avidor-Reiss *et al.*, 2004). Although these proteins were not detected in purified IFT particles, they are present in the membrane + matrix fraction of *Chlamydomonas* flagella (Pazour *et al.*, 2005). The only exceptions are the IFT122 and the PIFTC3 proteins that were not detected in that analysis (Figure 1).

Localisation of endogenous and tagged IFT proteins in mature and elongating flagella

To determine the location of IFT proteins in trypanosomes, mouse polyclonal antibodies were raised against a classic IFT marker, the IFT172 protein. It has been localised to the flagellum matrix and to the basal bodies of *Chlamydomonas* where it is required for flagellum assembly (Pedersen *et al.*, 2005) as well as in *C. elegans* (Bell *et al.*, 2006). It is also involved in hedgehog signalling in mouse (Huangfu *et al.*, 2003). A fragment of the

trypanosome *IFT172* gene was expressed in *E. coli* to produce a fusion protein with the glutathione-S-transferase (GST) for injection in mice. In a second approach, the genes encoding IFT20 or IFT52 were selected for fusion to a protein A tag (Estevez *et al.*, 2001) or to GFP, respectively. IFT20 and IFT52 are proteins belonging to the B complex that have been well characterised in *Chlamydomonas* (Deane *et al.*, 2001), *C. elegans* (Collet *et al.*, 1998) or in mammalian cells (Follit *et al.*, 2006). The expression of the fusion proteins is controlled by a tetracycline-inducible promoter and is activated by addition of tetracycline to the culture medium. Western blot analysis with an anti-protein A antibody or with an anti-GFP antibody confirmed that the IFT20 tagged protein and the GFP::IFT52 protein are expressed upon addition of tetracycline and show an electrophoretic motility corresponding to the expected size of the fusion protein (Figure S1A,B).

Indirect immuno-fluorescence assay (IFA) with anti-IFT172 antibodies produced a defined pattern on trypanosomes fixed in methanol: a strong signal is observed at the basal body region and a succession of closely spaced spots is found all along the length of the flagellum until its distal tip (Figure 2A). The same pattern was observed in cells possessing two flagella and no visible difference in signal could be detected between the new (no matter its length) and the old flagellum (see for example the cell at the bottom left of Figure 2A). The same antiserum used on PFA-fixed trypanosomes stained the flagellar compartment but not the basal body (data not shown), possibly due to a more difficult access as previously noted for IFT20 in mammalian cells (Follit *et al.*, 2006). IFT20 fused to a protein A tag also localised to the flagellum and to the basal body, with a weak signal on the cell body (Figure 2B). Double staining with markers of various organelles (endoplasmic reticulum, lysosomes, mitochondria) failed to reveal a specific association, indicating that the protein is present in the cytosol, possibly as a consequence of over-expression (Figure S1C,D and data not shown). Finally, observation of live cells expressing GFP::IFT52 also demonstrated localisation to the

basal body and the pro-basal body and to the flagellar compartment of both old and new flagellum, with a more pronounced localisation at the proximal part of the flagellum (data not shown). This pattern was preserved after methanol fixation, although it became less intense (Figure 2C). Staining with an anti-GFP antibody confirmed this localisation (Figure S1F,G).

To further investigate IFT proteins, trypanosomes were treated with 0.1 % Nonidet-P40 prior to fixation. Detergent addition removes the cell body and flagellum membranes but the subpellicular corset of microtubules, the axoneme, the PFR and the basal body complex remain intact (Sherwin and Gull, 1989). Detergent treatment abolishes most of the flagellum staining for IFT172, tagged IFT20 and GFP::IFT52 but a clear signal remains present at the basal body region in both methanol- and PFA-fixed cells (Figure 2D-F). This indicates that a pool of IFT172 with possibly different biochemical characteristics is present around the basal bodies, as recently suggested for Bardet-Biedl Syndrome (BBS) proteins (Nachury *et al.*, 2007).

To further define the positioning of IFT proteins, GFP::IFT52 expressing cells were stained with several markers of the basal body (Figure 3A-D). Double labelling with MAb22, a monoclonal antibody marker of the proximal region of both mature and pro basal bodies (Pradel *et al.*, 2006; Absalon *et al.*, 2007) showed that GFP::IFT52 was found in a more apical position (Figure 3A), a feature that was reproduced for tagged IFT20 (Figure S1E). The antibody against TBBC (Trypanosome Basal Body Component, (Dilbeck *et al.*, 1999)), a protein found exclusively on the mature basal body that hence produces a single spot in IFA (S.A. et al., manuscript in preparation) showed that GFP::IFT52 was present in an even more apical position (Figure 3B). Co-staining was also performed with two antibodies against centrins, that localise to mature and pro-basal bodies, as well as to a “bi-lobed” structure found close to the Golgi apparatus (He *et al.*, 2005; Selvapandiyan *et al.*, 2007). The monoclonal antibody 20H5 recognises numerous centrin proteins from different organisms

and in detergent-extracted trypanosomes was found to light up the flagellum, the mature and the pro-basal body as well as a structure close to the flagellar pocket and the Golgi apparatus (Figure 3C). A similar pattern was obtained with the antiserum raised against centrin 1 from the related organism *Leishmania donovani*, except that the flagellum and basal body signals were weaker (Figure 3D). In both cases, GFP::IFT52 was found to merge with the centrin signal at the mature basal body. The relative position of IFT proteins themselves was investigated upon staining of GFP::IFT52 expressing cells with the anti-IFT172 antiserum, revealing a close but separate location for the two proteins. GFP::IFT52 was found to be in a more apical location compared to IFT172 (Figure S2). Double staining of tagged IFT20 expressing cells with the anti-protein A antibody and the anti-IFT172 antiserum showed that these two proteins co-localised at the basal body region (Figure S2).

In conclusion, three different IFT proteins are present along the length of the axoneme where they are sensitive to detergent, and at the mature basal body and frequently at the pro-basal body where they are resistant to detergent. Importantly, they localise to both old and new flagella, indicating that IFT could operate in mature and elongating flagella.

Movement of GFP::IFT52 protein in trypanosome flagella

Presence of various IFT proteins in both old and new flagella does not necessarily prove that these proteins are trafficking in this compartment. We therefore examined the behaviour of the GFP::IFT52 fusion protein in live trypanosomes. Agarose was added to the medium to restrict cell movement and direct GFP fluorescent signals were monitored by video-microscopy. This showed unambiguous movement of fluorescent particles in flagella, providing the first actual evidence for intraflagellar transport in trypanosomes (Supplementary Videos 1-2, still images of movie 1 are presented at Figure 3F). Intraflagellar movement was detected in both old and new flagella, but was more difficult to quantify on the new flagellum

as this one is regularly found on top of the cell body, which tends to obliterate the fluorescent signal. IFT was best visualised on the distal end of the mature flagellum (Movies S1-2) but was also detected in the new flagellum when it lied on the side of the cell (Movie S1). Anterograde events were more frequent and easier to observe (Movies S1-S2) but a few retrograde events could also be detected (Movie S2). Rate of anterograde IFT was measured at ~3 $\mu m.sec^{-1}$. Retrograde transport was faster but could not be estimated accurately due to its low frequency and to the weak GFP signal. These data demonstrate that IFT is indeed active in trypanosomes and operates in both mature and assembling flagella.

IFT-like particles in the trypanosome flagellum

In *Chlamydomonas*, IFT particles can be recognised on flagellum sections as electron-dense granules found between the membrane and the axoneme (Kozminski *et al.*, 1993). Occasional viewing of such particles has been previously reported in *T. brucei* but detailed analysis is lacking (Bastin *et al.*, 2000b). We examined a large number of cross-sections of flagella from wild-type and several RNAi motility mutants (Branche *et al.*, 2006) and noticed the frequent presence of granule-like structures with a diameter of 20-30 µm (Figure 4A-F & Figure S3 of Supplemental Material). Usually only one particle is visible per section (Figures 4A and 4C) but in rare instances (< 5 %), several particles can be seen on the same section (Figure 4B). Remarkably, particles show a very specific location relative to the axoneme doublets (Figure 4D): they are either associated to doublets 3-4 (Figure 4A) or 7-8 (Figure 4C) but are never found next to doublets 5 to 6, doublet 9 and rarely close to doublets 1 and 2 (Figure 4D). Longitudinal sections showed that the particles look like flat rafts with one side that is very close to the microtubules and the other that appears almost in contact with the flagellar membrane (Figure 4E). Presence of the IFT-like particles seems to position the flagellar membrane more closely towards the axonemal microtubules (Figure 4E).

We also looked at flagellum sections of RNAi mutants where expression of two proteins of the central pair (PF16 or PF20) had been separately silenced, leading to inhibition of motility but without interfering with flagellum construction (Branche *et al.*, 2006; Ralston *et al.*, 2006). Similar particles are visible in these flagella (Figure 4C) although at a slightly lower frequency: 31 % of sections for $PF16^{RNAi}$ cells and 24 % for $PF20^{RNAi}$ cells instead of 57 % for wild-type (Figure 4L). Nevertheless, they all show the preferential association to the same doublets as was found in wild-type cells (Figure 4D).

As the new flagellum is always found in the same position relative to the old one (Briggs *et al.*, 2004b), it can be identified in the few sections where both flagella are clearly visible. This revealed that both flagella contain these particles (a clear example for the old flagellum is shown at Figure 4F). IFT-like particles are never recognised in the transition zone of the basal body, although some amorphous, relatively electron-dense, material is visible between the microtubule doublets and the membrane (Figure 4G). This was clearly different from the inside of the axoneme shaft that appear much more translucent (Figure 4G). The central pair and the dynein arms are already visible in flagellum sections close to the top of the flagellar pocket (as confirmed by the short diameter of the flagellar pocket lumen). The PFR is not yet present but a large amount of material is found around the microtubule doublets, sometimes resembling the granules identified above (Figure 4H-I).

Detergent-treatment suppresses most of the IFT172, tagged IFT20 or GFP::IFT52 signal at the flagellum. To relate this result with granules seen by electron microscopy, wild-type, $PF16^{RNAi}$ or $PF20^{RNAi}$ cells were treated with 1 % Nonidet P-40. This procedure removes the cell membrane but ensures an excellent conservation of the whole trypanosome cytoskeleton for electron microscopy analysis, including the axoneme and the PFR (Sherwin and Gull, 1989). In these conditions, the frequency of IFT-like particles drops, with less than 10 % of samples showing a possible remnant at the expected position on doublets 3-4 or 7-8

(Figures 4J-L). This result shows that these granules display the same characteristics as the three IFT proteins studied above.

IFT *genes are necessary for flagellum construction*

Expression of the trypanosome genes *IFT122, IFT140* (complex A) and *IFT20, IFT52, IFT55, IFT80, IFT88, IFT172* (complex B) was individually silenced by inducible RNAi in trypanosomes and knock-down efficiency was controlled at the RNA level by semi-quantitative RT-PCR (Figure S4). In all cases, RNAi silencing led to the inhibition of new flagellum formation and to the emergence of apparently non-flagellated trypanosomes (Figure 5A-B). However, the old flagellum is not depolymerised and remains present. Analysis of cells fixed at different stages of RNAi silencing followed by IFA staining using a monoclonal antibody recognising a major PFR protein (Figure 5A-B) showed a mixture of different cell types: cells retaining the old flagellum, cells with a shorter flagellum and cells without PFR signal, that could correspond to cells with very short flagella missing the PFR or to non-flagellated cells (see below). Cells with shorter flagella exhibited a reduced cell size, with those without a visible flagellum being the shortest ones (Figures 5A-B), in agreement with the central role of the flagellum in the definition of cell size (Kohl *et al.*, 2003).
Trypanosomes are difficult to synchronise reliably, meaning that RNAi induction is likely to have different effects according to the position of a cell in its cycle. It is therefore important to examine carefully cells throughout the induction. IFA with the anti-PFR was first used to score proportions of positive and negative cells during the course of RNAi silencing of *IFT* and genes (Figure 5D-E). Significant differences were noted in the rate of emergence of non-flagellated cells. In the case of complex A proteins, knock-down of IFT140 leads to faster emergence of non-flagellated cells compared to IFT122 (Figure 5D). Differences are also observed in the case of knock-down of RNA encoding complex B proteins. For example, it

takes only 30 hours to obtain 50 % of non-flagellated cells during silencing of *IFT172* whereas it takes an extra 40 hours to generate a similar result for *IFT52* knock-down (Figure 5E). Hence, these differences in kinetics are not linked to genes encoding members of a specific complex. Inhibition of any of the *IFT* genes invariably leads to a growth arrest whose timing is correlated with the kinetics of emergence of non-flagellated cells (Figure 5D,G and 5E,H for proteins of complex A and B, respectively). For example, in the case of complex A members, silencing of IFT140 rapidly produces a large number of non-flagellated cells and leads to a more premature growth arrest compared to *IFT122*^{RNAi} grown and induced in the same conditions (Figure 5G).

These differences in kinetics could reflect variable efficiency of RNA destruction or different rates of protein turn-over (or both). RT-PCR analysis was performed on total RNA extracted from cell lines non-induced or induced for up to 5 days. Abundance of each target RNA was normalised with a control unrelated mRNA (Figure S4). Kinetics of RNA silencing are very reproducible for all RNAi cell lines investigated: a potent silencing is observed 2 days after induction and a slight increase in the amount of the target RNA is noted the following days. This reproduces kinetic patterns observed for other RNAi cell lines developed in separate experiments (M. Durand-Dubief, S.A. & P.B., manuscript in preparation). In summary, the differences in kinetics of emergence of non-flagellated cells during the course of RNAi are not due to a variable efficiency of RNA degradation but are likely to reflect differences at the protein level.

Distinct phenotype upon silencing of genes required for anterograde or retrograde transport

In *Chlamydomonas* and *C. elegans*. inhibition of proteins associated to anterograde transport (IFT B and kinesin II complexes) leads to complete or severe inhibition of flagella

or cilia formation. By contrast, blocking of retrograde transport (IFTA and dynein complexes) produces short cilia or flagella, filled with IFT material that can penetrate the flagellar compartment but cannot be recycled to the base (Cole, 2003). We analysed *IFT88*^{RNAi} (mutant of a complex B protein) and *IFT140*^{RNAi} (mutant of a complex A protein) induced cells by double staining with the anti-IFT172 antiserum as a marker of the IFT particles and with the MAb25 antibody as a marker of the axoneme (Figures 6A-C & 6E). In the case of *IFT88*^{RNAi}, the majority of short cells did not exhibit a flagellum (no MAb25 signal) and only showed a weak signal for IFT172, indicating that absence of IFT88 severely blocks flagellum formation and leads to a reduction or a dispersion of IFT172 (Figure 6A, stars & Figure 6C). This result was supported by scanning electron microscopy that revealed that most short cells did not exhibit a flagellum. In the rare cases where a flagellum could be detected, it often appeared short (less than 1 µm) and thin (Figure 6D). Cells that retained the old flagellum were still positive for both the MAb25 axoneme marker and the anti-IFT172, no matter the length of the flagellum (Figure 6A, arrows for long flagellum and arrowheads for flagella of intermediate lengths). A very different result was obtained for the *IFT140*^{RNAi} cells stained with the same antibodies (Figures 6B & 6E). Numerous short cells were seen with a short line as MAb25 signal, indicating formation of a short axoneme, and with a very intense signal for IFT172 (Figures 6B, star & Figure 6E). The presence of short flagella filled with IFT172 proteins, producing very bright spots of fluorescence, increased rapidly during the course of RNAi silencing, whereas it was virtually never detected in the case of *IFT88*^{RNAi} (Figure 6G). Scanning electron microscopy demonstrated the presence of cells with short flagella (1-3 µm) with large dilations (Figure 6F), that very likely results from the accumulation of IFT proteins. However, cells that retained an old flagellum of normal length still exhibited the usual MAb25 and anti-IFT172 signals (Figure 6B, arrows). By contrast,

cells that possessed a flagellum of intermediate length (around 5 µm) showed normal MAb25 signal but much increased abundance of IFT172 protein (Figure 6B, arrowhead).

Although construction of the new flagellum is inhibited or strongly reduced, the old flagellum remains present and is still motile. We examined *IFT140*^{RNAi} cultures at early stages of RNAi, with special emphasis on cells that were binucleated, so at late stages of their cell cycle (Figure 6H). The mature flagellum was normal and exhibited the expected signal for the anti-IFT172 antiserum whereas the new flagellum was very short and filled with IFT172 protein. This shows that the old and the new flagellum are independent from each other and despite the arrest of new IFT140 production, IFT140 protein present in the old flagellum is still functional. The ultra-structure of the old flagellum of *IFT88*^{RNAi} and *IFT172*^{RNAi} (anterograde transport mutants) and *DHC1b*^{RNAi} (retrograde transport mutant) was examined by transmission electron microscopy. Induction times were selected in such a way that cells were at a stage when they had stopped constructing a new flagellum, so that almost all flagellar sections should correspond to the old flagellum. This was carried out on whole cells and detergent-extracted cytoskeletons (Figure S3). Sections through flagella were less frequent on induced cells compared to wild-type or non-induced controls, as expected from the drop in the proportion of flagellated cells upon RNAi induction. However, the ultra-structure of the axoneme appeared intact: the 9 doublets microtubules, the central pair, the dynein arms and radial spokes were all present (Figure S3). Their flagellar pocket also appeared structurally normal, as well as the flagellum adhesion zone (Figure S3). Importantly, IFT particles are still visible on the old flagellum (Figure S3). We observed IFT-like particles on 6 out of 19 such profiles, i.e. a proportion similar to that observed for populations of cells that build their flagellum normally, indicating that IFT particles remain present in the old flagellum. This is confirmed by IFA with the anti-IFT172 that still stains the

old flagellum of *IFT140*^{RNAi} (Figure 6H), *IFT88*^{RNAi} and *DHC1b*^{RNAi} (data not shown) cells induced for 2 or 3 days, indicating a slow turn-over of IFT proteins in mature flagella.

Transmission electron microscopy was used to examine the new flagellum in control wild-type cells or *IFT88*^{RNAi} and *DHC1b*^{RNAi} cells (Figure 7). The basal body is rooted within the cell body whereas the transition zone is covered by the flagellum membrane and localised in the lumen of the flagellar pocket of wild-type cells (Figure 7A). The latter one exhibits a typical asymmetric structure with the larger lumen side found at the anterior end. When a new flagellum is assembled, it is made in the same flagellar pocket (Grasse, 1961) found on the large, anterior, side of the lumen (arrow on Figure 7B). The transition zone is clearly recognisable and a mass of amorphous material is found at the distal growing end (Figures 7B-C), wrapped by the flagellum membrane that sometimes appears distorted (Figures 7B). The basal bodies of such flagella are "bald", i.e. axoneme microtubules have not yet elongated. These basal bodies appear shorter, suggesting that they have not fully matured yet. This was encountered in 5 out of the 72 analysed sections of the flagellar pocket (7 %)(Table 1). The new flagellum grows and axoneme microtubules are now visible in continuity with those of the transition zone. Nevertheless, this new flagellum remains in the same flagellar pocket as the old flagellum (Fig 7D). In non-synchronous cultures of wild-trypanosomes, 16 % of flagellar pockets contain two flagella (n=72). Finally, two individual flagellar pockets are visible, each containing a single flagellum (Figure 7E).

Ultra-structure of the basal body and the flagellum was analysed in *IFT88*^{RNAi}, *IFT172*^{RNAi} (mutants of anterograde transport) and *DHC1b*^{RNAi} (mutant of retrograde transport) cells at induction times where assembly of the new flagellum is drastically reduced (Figures 7F-I). Longitudinal sections through basal bodies were grouped in three categories: those where axonemal microtubules are visible in direct continuity of the transition zone and appear normal, those where axonemal microtubules are present but interrupted and those

where only a bald basal body is visible (Table 1). In all *IFT*^{RNAi} mutants analysed, the frequency of bald basal bodies rose significantly reaching close to 80 % in the *IFT88*^{RNAi} cell line (Table 1). Some material is frequently detected on top of the basal body and looks like flagellar membrane extension (see below) but it does not resemble to what was observed for wild-type flagella (compare Figure 7F with 7B-C). The proximal region of all basal bodies still exhibits triplet microtubules and the transition zone looks apparently normal. Nevertheless, these basal bodies appear slightly shorter, like the basal bodies of short new flagella in wild-type cells (Figure 7B-C). These data demonstrate that axoneme formation is strongly inhibited in the absence of a protein of the IFT B complex. In the case of *DHC1b*^{RNAi} cells, about half of the sections revealed the presence of a bald basal body but other situations were also encountered. Large accumulation of electron-dense material resembling IFT particles was observed (Figure 7H). Moreover, several sections showed the presence of short microtubules and some material trapped between this axoneme and the tip of the flagellar membrane (Figure 7I). In these situations, the basal body displayed a normal length. This accumulation fits with the dilation of short flagella of retrograde transport mutants observed by scanning electron microscopy and by IFA with the anti-IFT172 antiserum (Figure 6).

We conclude that in the absence of retrograde transport, members of the IFT complex B can still access the flagellum and accumulate there as they cannot be recycled due to the absence of retrograde activity. This would allow the formation of short and dilated flagella. Conversely, in the absence of anterograde transport, entry of IFT protein in the flagellum is restricted and flagellum formation is more strongly inhibited.

PIFT *genes are required for flagellum construction and can be classified as involved in anterograde or retrograde transport*

Expression of *PIFT* genes was knock-downed by RNAi and monitored in parallel to the mutants of conventional *IFT* genes, revealing that all 5 selected *PIFT* genes were required for flagellum formation (Figure 5C, F). Significant differences were also observed in the emergence of non-flagellated cells (Figure 5F), with fast phenotypes for silencing of *PIFTA1, PIFTB2* or *PIFTC3* (50 % non-flagellated cells in 48-60 hours) and the slower kinetics for *PIFTF6* knock-down (50 % of non-flagellated cells after 120 hours of induction) and *PIFTD4* (3-5 % of non-flagellated cells after 120-240 hours of induction, data not shown). These differences correlated with the timing of growth arrest (Figure 5I, see Figure S5A,B for $PIFTF6^{RNAi}$), as observed in the case of silencing conventional *IFT* genes (Figures 5G-H).

To evaluate the participation of these novel genes in IFT, IFA staining with the anti-IFT172 was performed on the 5 $PIFT^{RNAi}$ cell lines (Figure 8 and Figure S6). Flagellum presence and IFT172 signal were drastically reduced in $PIFTA1^{RNAi}$, $PIFTB2^{RNAi}$ and $PIFTC3^{RNAi}$. In the latter case, an increase of the cytoplasmic signal was consistently observed, indicating a possible redistribution of IFT172 in the cytoplasm (Figure 8B). In contrast, cells with short flagella brightly stained by the anti-IFT172 antiserum were abundant in $PIFTD4^{RNAi}$ and $PIFTF6^{RNAi}$ induced cells. Quantification of the proportion of short cells with bright, weak or no IFT172 signal was performed on all 5 $PIFT^{RNAi}$ cell lines and revealed that $PIFTA1^{RNAi}$, $PIFTB2^{RNAi}$ and $PIFTC3^{RNAi}$ behave similarly to $IFT88^{RNAi}$ (complex B) whereas $PIFTD4^{RNAi}$ and $PIFTF6^{RNAi}$ behave similarly to $IFT140^{RNAi}$ (complex A) (Figure 8D). Scanning electron microscopy demonstrated that when visible, short flagella of $PIFTA1^{RNAi}$ were smaller and thinner compared to those from $PIFTD4^{RNAi}$ or $PIFTF6^{RNAi}$ (Figure S6). These results support the hypothesis that PIFTA1, PIFTA2 and PIFTC3 proteins are involved in anterograde transport whereas PIFTD4 and PIFTF6 are involved in retrograde transport.

Flagellar membrane extension can take place in the absence of IFT

While analysing *IFT*^{RNAi} cells by scanning electron microscopy, we frequently noticed the presence of membrane extensions of various length and shape. To understand the signification of this phenotype, glutaraldehyde-fixed samples from *IFT20*^{RNAi}, *IFT172*^{RNAi} (complex B), *IFT140*^{RNAi} (complex A), *PIFTA1*^{RNAi} and *PIFTF6*^{RNAi} cell lines at various stages of RNAi silencing were investigated (Figure 9). At least 5 categories of short cells could be defined and their proportion was quantified in the various RNAi cell lines analysed (Figure 9A-B): (1) "smooth" cells with no visible flagella nor other recognisable structures (however these could be hidden at the other face of the sample)(Figure 9Aa); (2) cells without flagella but with an unusual surface "depression" that might correspond to an 'empty' flagellar pocket (identification is difficult without specific markers)(Figure 9Ab,c); (3) cells with a 'filament' that is often resolved as a close succession of small 'balls' or sometimes as large vesicles that emerge from a depression without recognisable flagellar structure (yellow arrowheads on the Figure 9Ad); (4) short flagella (yellow arrow) alone (Figure 9Ae) and (5) short flagella with a thin extension (Figure 9Af). This last case could correspond to the "flagellar sleeve", an amazing, long and thin extension of the flagellar membrane described for short flagella of the *IFT80*^{RNAi} mutant (Davidge *et al.*, 2006).

As induction of RNAi silencing goes on, the proportion of cells with a short flagellum drops rapidly (Figure 9B). This drop is more severe in the case of knock-down of members of the IFT complex B (IFT20 and IFT172, less than 25 % of flagellated cells) and of PIFTA1 compared to complex A (IFT140, close to 50 % of flagellated cells) or PIFTF6 (Figure 9B). Cells with a flagellar 'sleeve' were observed in all *IFTRNAi* and *PIFTRNAi* mutants, as well as in the *DHC1b*^{RNAi} mutant, indicating that this is a consequence of inhibition of flagellum formation rather than an phenotype specific to IFT80 (Davidge *et al.*, 2006)(Figure 9). Examination of cells that still possess an old flagellum demonstrated that when a new short

flagellum is still visible, the flagellar sleeve is present starting from the distal tip of this flagellum and connecting to the old flagellum, presumably at the position of the flagellar connector, a structure that links the tip of the new flagellum to the side of the old one (Moreira-Leite *et al.*, 2001; Kohl *et al.*, 2003; Davidge *et al.*, 2006) (Figures 9C, S5C and S6). When no new flagellum was visible, a succession of vesicle-like structures was found at the expected location of the flagellar sleeve (Figure S6C). Transmission electron microscopy confirmed that these vesicles emanate from the flagellar pocket and adhere to the cell surface (Figure 9C). These results indicate that inhibition of axoneme construction does not prevent flagellum membrane elongation. This was observed in anterograde transport mutants despite the total inhibition of axoneme assembly (Figure 7F where only a bald basal body is present). These results suggest that separate pathways are acting for formation of the cytoskeletal and the membrane compartment of the flagellum (Davidge *et al.*, 2006).

DISCUSSION

IFT in flagellum construction and maintenance

This work provides the first actual demonstration of intraflagellar transport in *T. brucei* and reveals the activity of this process in both old and new flagella. Three different IFT proteins were found in old and new flagella using different methodologies: IFA with antibodies raised against an endogenous protein (IFT172), expression of tagged protein followed by IFA (IFT20) and direct visualisation of an expressed GFP fusion protein (IFT52). IFT particles were identified by transmission electron microscopy between the axoneme doublets and the flagellum membrane. These particles and the IFT proteins found in the flagella are lost upon detergent-treatment that removes the membrane of the flagellum, in agreement with protein complexes that are displaced and are not tightly associated to microtubules. This is further supported by the absence of all IFT and PIFT proteins studied here from the proteomic analysis of *T. brucei* flagella purified with detergent and high-salt concentrations (Broadhead *et al.*, 2006).

The restricted location of IFT particles to two sets of specific doublet microtubules (3-4 and 7-8) could be partially explained by physical constraints resulting from the presence of the PFR. This large extra-axonemal structure runs along the axoneme from its point of emergence from the flagellar pocket until its distal tip and is tightly linked to the axoneme *via* physical connections to microtubule doublets 4 to 7 (Bastin *et al.*, 1996). This could interfere with movement of molecular motors and their cargo along microtubules. However, it does not explain why particles are so infrequent close to doublets 1, 2 and 9. As IFT particles travel in both directions in the flagella, we propose that some doublets serve as specific tracks for anterograde or retrograde transport exclusively, hence reducing the risk of collision and offering the opportunity for precise regulation of each set of motor.

Movement of GFP::IFT52 particles has been visualised in both directions, anterograde tracks being much more abundant. In *Chlamydomonas*, particles trafficking from tip to base are smaller than those travelling in the opposite direction (Kozminski *et al.*, 1993). If the same was true in trypanosome, retrograde IFT particles could be at the limit of detection. IFT rates are closer to what was reported for *Chlamydomonas* (Kozminski *et al.*, 1993) compared to *C. elegans* (Orozco *et al.*, 1999) or to primary cilia of mammalian cells (Follit *et al.*, 2006). Faster IFT could be linked to (1) longer flagella (10 µm for *Chlamydomonas* and and 20 µm for *T. brucei*, compared to 3 to 6 µm for the analysed mammalian or *C. elegans* cilia) and/or to (2) motile axoneme, where several structures made of protein complexes such as dynein arms and radial spokes are transported for assembly (Qin *et al.*, 2004). Functional studies will be required to understand the reasons for these differences. In Trypanosomatids, two distinct genes encode IFT dynein heavy chains (Adhiambo *et al.*, 2005) and functional analysis indicates that both are required for retrograde IFT (our unpublished data).

In addition to the flagellum compartment, IFT proteins are also abundant at the base of the flagellum where they localise to the apical region of the basal body. By contrast to IFT proteins in the flagellum, these proteins are resistant to detergent-extraction of the cytoskeleton. This suggests different biochemical properties and could be explained if proteins were sequestered in a complex at the base of the flagellum, as proposed for BBS proteins (Nachury *et al.*, 2007). A slightly different localisation was noted for GFP::IFT52, that appears in a more apical position compared to IFT20 or IFT172. In green algae, IFT52 localises to fibres that delimitates the flagellum and the cell body cytoplasmic compartments (Deane *et al.*, 2001). Different localisations for IFT proteins in the basal body region have also been reported in *Chlamydomonas* (Hou *et al.*, 2007).

Importantly, both old and new flagella possess equal concentration of IFT proteins showing the presence of IFT in an organelle that is either in construction (the new one) or in

maintenance (the old one) in the same cell. When the new flagellum is assembled, incorporation of new subunits take place at its distal tip while only a small amount of material is turned over in the old flagellum (Bastin *et al.*, 1999a). The presence of IFT material in both flagella indicates that this differential targeting is not due to more prominent IFT activity in the new flagellum.

Knock-down of each individual *IFT* or *PIFT* gene leads to a potent inhibition of elongation of the new flagellum but without a visible effect on the existing flagellum, as initially reported for *IFT88* and *DHC1b* (Kohl *et al.*, 2003) and recently for *IFT80* (Davidge *et al.*, 2006). Duplication of the basal body is not affected as confirmed by the presence of a short new basal body in all IFT^{RNAi} cell lines analysed. However, elongation appears more limited. In the case of mutants of retrograde transport (complex A proteins IFT122 and IFT140, DHC1b dynein motor), short flagella can still be assembled in many cells but axoneme microtubules failed to elongate extensively and IFT material accumulates in the flagellar compartment. A similar situation has been encountered in the DHC1b mutants of *Chlamydomonas* (Pazour *et al.*, 1999; Porter *et al.*, 1999) and of *C. elegans* (Signor *et al.*, 1999) where retrograde transport is also blocked. No mutants of complex A has been reported to date in the green algae whereas cilia of worms lacking functional proteins of this complex also accumulate IFT proteins (Blacque *et al.*, 2006). However, they are only slightly shorter (~4 µm) compared to wild-type cilia (~6 µm). Inhibition of proteins of the B complex leads to strong inhibition of flagellum or cilium formation in trypanosomes as in *Chlamydomonas*, *C. elegans* (Rosenbaum and Witman, 2002) or *Tetrahymena* (Brown *et al.*, 2003), showing the functional conservation of this process.

In *Chlamydomonas*, transfer of thermo-sensitive mutants at the restrictive temperature leads to inactivation of kinesin II within existing flagella, revealing the role of IFT in both flagellum construction and maintenance (Kozminski *et al.*, 1995). In RNAi silencing, only

RNA is targeted and existing proteins are lost according to their turn-over rate (Bastin *et al.*, 2000a). A constant feature in RNAi silencing of *IFT* genes in trypanosomes is the persistence of the old flagellum despite the total block in new flagellum formation. Two explanations can be proposed: (1) IFT is not required for flagellum maintenance and (2) IFT proteins engaged in old flagella maintenance are turned-over very slowly. Old flagella in wild-type contain IFT particles and IFT proteins, supporting the second hypothesis. Video-microscopy revealed similar trafficking of GFP::IFT52 in old and new flagella, showing that IFT activity is not slowed down in the old flagellum. In the case of induced IFT^{RNAi} cells, the persisting old flagella still beat and conserve an apparently normal ultra-structure with the 9+2 arrangement, dynein arms and radial spokes. A possible clue to explain this situation could lie in the formation of new flagella in normal cells: they incorporate a large amount of IFT-like material in the flagellar compartment, even before the beginning of axonemal microtubule polymerisation, a feature previously reported in *Trypanosoma equiperdum* (Grasse, 1961). This has been observed in *Chlamydomonas* where short flagella are filled with IFT material that is progressively spread out along the length of the flagellum (Marshall and Rosenbaum, 2001; Dentler, 2005; Marshall *et al.*, 2005). A flagellum could be assigned a defined amount of IFT protein prior to assembly and these proteins would circulate within this flagellum compartment with possible exchange with IFT proteins at its basal body but not with the rest of the cytoplasm (and hence not with the new basal body complex). This could explain why RNAi silencing does not reduce significantly the amount of IFT material in the old flagellum and thereby the remarkable long-life of this flagellum.

PIFT proteins are required for flagellum formation

The 5 *PIFT* genes identified by comparative genomics all turned out to be essential for flagellum formation, indicating the usefulness of this approach, also applied to identify genes

involved in flagellum beating (Baron *et al.*, 2007). The PIFT proteins are likely linked to anterograde or retrograde transport, as reported recently for the corresponding genes in *C. elegans* (Blacque *et al.*, 2005; Murayama *et al.*, 2005; Blacque *et al.*, 2006; Efimenko *et al.*, 2006). These genes are conserved in *Chlamydomonas*, but their encoded proteins are not purified with IFT particles. This could be explained by a lower stoechiometry in the IFT particle or a weaker association that could be disrupted during purification. Alternatively, PIFT proteins could function in assembly or remodelling of the IFT particle without being a structural component *per se*.

Membrane trafficking to the trypanosome flagellum

In addition to axoneme and PFR components, a significant amount of membrane is required to construct a flagellum. It has been proposed that vesicles are targeted to the base of the flagellar compartment to deliver both membranes and membrane proteins (Rosenbaum and Witman, 2002). In trypanosomes, all trafficking takes place in the flagellar pocket, the only site for endocytosis and exocytosis. Our results show that in the absence of a new flagellum, a flagellar pocket structure remains associated to the bald basal body. This was first noticed by Davidge *et al*. (2006) who recently reported that a "flagellar sleeve" was extending from the basal body region of $IFT80^{RNAi}$ induced cells, passing through the neck of the pocket and whose tip would be maintained on the existing flagellum by the flagellar connector, a structure that holds the distal end of the new flagellum to the side of the old one (Moreira-Leite *et al.*, 2001). The flagellar sleeve was visible in the 7 IFT^{RNAi} or $PIFT^{RNAi}$ mutants examined here, but intermediate structures with succession of vesicles were as frequent. This shows that despite the absence of IFT activity and of microtubule elongation, a flagellar compartment is still defined.

Acknowledgements

We thank M. Bonhivers and D.R. Robinson for providing antibdoies prior to publication and for numerous discussions, A. Estevez for advise on the tap-tag system, J. Beisson, G. Cross, P. Englund, K. Gull, P. Michels and H. Nakhasi for providing trypanosome cell line, plasmids or various antibodies. We acknowledge the electron microscopy departments of the Muséum National d'Histoire Naturelle and of the Pasteur Institute for providing access to their equipment, as well as advises from M.C. Prévost, N. Cayet and S. Guadagnini. This work was funded by the CNRS, by a Programme Protéomique et Génie des Protéines (D. Robinson & PB), an ACI grant in Development Biology, by a GIS grant on rare genetic diseases (PB) and by Sanofi-Aventis. S.A. was funded by a MRT, FRM and Pasteur-Weizmann fellowships. D.J. is funded by an ANR grant "Maladies Rares" and by a Roux fellowship.

References

Absalon, S., Kohl, L., Branche, C., Blisnick, T., Toutirais, G., Rusconi, F., Cosson, J., Bonhivers, M., Robinson, D., and Bastin, P. (2007). Basal Body Positioning Is Controlled by Flagellum Formation in *Trypanosoma brucei*. PLoS ONE *2*, e437.

Adhiambo, C., Forney, J.D., Asai, D.J., and LeBowitz, J.H. (2005). The two cytoplasmic dynein-2 isoforms in *Leishmania mexicana* perform separate functions. Mol Biochem Parasitol *143*, 216-225.

Avidor-Reiss, T., Maer, A.M., Koundakjian, E., Polyanovsky, A., Keil, T., Subramaniam, S., and Zuker, C.S. (2004). Decoding cilia function: defining specialized genes required for compartmentalized cilia biogenesis. Cell *117*, 527-539.

Baron, D.M., Ralston, K.S., Kabututu, Z.P., and Hill, K.L. (2007). Functional genomics in *Trypanosoma brucei* identifies evolutionarily conserved components of motile flagella. J Cell Sci *120*, 478-491.

Bastin, P., Ellis, K., Kohl, L., and Gull, K. (2000a). Flagellum ontogeny in trypanosomes studied via an inherited and regulated RNA interference system. J Cell Sci *113*, 3321-3328.

Bastin, P., MacRae, T.H., Francis, S.B., Matthews, K.R., and Gull, K. (1999a). Flagellar morphogenesis: protein targeting and assembly in the paraflagellar rod of trypanosomes. Mol Cell Biol *19*, 8191-8200.

Bastin, P., Matthews, K.R., and Gull, K. (1996). The paraflagellar rod of kinetoplastida: solved and unsolved questions. Parasitol Today *12*, 302-307.

Bastin, P., Pullen, T.J., Moreira-Leite, F.F., and Gull, K. (2000b). Inside and outside of the trypanosome flagellum:a multifunctional organelle. Microbes Infect *2*, 1865-1874.

Bastin, P., Pullen, T.J., Sherwin, T., and Gull, K. (1999b). Protein transport and flagellum assembly dynamics revealed by analysis of the paralysed trypanosome mutant snl-1. J Cell Sci *112*, 3769-3777.

Bastin, P., Sherwin, T., and Gull, K. (1998). Paraflagellar rod is vital for trypanosome motility. Nature *391*, 548.

Bell, L.R., Stone, S., Yochem, J., Shaw, J.E., and Herman, R.K. (2006). The molecular identities of the *Caenorhabditis elegans* intraflagellar transport genes dyf-6, daf-10 and osm-1. Genetics *173*, 1275-1286.

Berriman, M., et al. (2005). The genome of the African trypanosome *Trypanosoma brucei*. Science *309*, 416-422.

Blacque, O.E., Li, C., Inglis, P.N., Esmail, M.A., Ou, G., Mah, A.K., Baillie, D.L., Scholey, J.M., and Leroux, M.R. (2006). The WD repeat-containing protein IFTA-1 is required for retrograde intraflagellar transport. Mol Biol Cell *17*, 5053-5062.

Blacque, O.E., et al. (2005). Functional genomics of the cilium, a sensory organelle. Curr Biol *15*, 935-941.

Branche, C., Kohl, L., Toutirais, G., Buisson, J., Cosson, J., and Bastin, P. (2006). Conserved and specific functions of axoneme components in trypanosome motility. J Cell Sci *119*, 3443-3455.

Briggs, L.J., Davidge, J.A., Wickstead, B., Ginger, M.L., and Gull, K. (2004a). More than one way to build a flagellum: comparative genomics of parasitic protozoa. Curr Biol *14*, R611-612.

Briggs, L.J., McKean, P.G., Baines, A., Moreira-Leite, F., Davidge, J., Vaughan, S., and Gull, K. (2004b). The flagella connector of *Trypanosoma brucei*: an unusual mobile transmembrane junction. J Cell Sci *117*, 1641-1651.

Broadhead, R., Dawe, H.R., Farr, H., Griffiths, S., Hart, S.R., Portman, N., Shaw, M.K., Ginger, M.L., Gaskell, S.J., McKean, P.G., and Gull, K. (2006). Flagellar motility is required for the viability of the bloodstream trypanosome. Nature *440*, 224-227.

Brown, J.M., Fine, N.A., Pandiyan, G., Thazhath, R., and Gaertig, J. (2003). Hypoxia regulates assembly of cilia in suppressors of *Tetrahymena* lacking an intraflagellar transport subunit gene. Mol Biol Cell *14*, 3192-3207.

Cole, D.G. (2003). The intraflagellar transport machinery of *Chlamydomonas reinhardtii*. Traffic *4*, 435-442.

Cole, D.G., Diener, D.R., Himelblau, A.L., Beech, P.L., Fuster, J.C., and Rosenbaum, J.L. (1998). *Chlamydomonas* kinesin-II-dependent intraflagellar transport (IFT): IFT particles contain proteins required for ciliary assembly in *Caenorhabditis elegans* sensory neurons. J Cell Biol *141*, 993-1008.

Collet, J., Spike, C.A., Lundquist, E.A., Shaw, J.E., and Herman, R.K. (1998). Analysis of osm-6, a gene that affects sensory cilium structure and sensory neuron function in *Caenorhabditis elegans*. Genetics *148*, 187-200.

Davidge, J.A., Chambers, E., Dickinson, H.A., Towers, K., Ginger, M.L., McKean, P.G., and Gull, K. (2006). Trypanosome IFT mutants provide insight into the motor location for mobility of the flagella connector and flagellar membrane formation. J Cell Sci *119*, 3935-3943.

Deane, J.A., Cole, D.G., Seeley, E.S., Diener, D.R., and Rosenbaum, J.L. (2001). Localization of intraflagellar transport protein IFT52 identifies basal body transitional fibers as the docking site for IFT particles. Curr Biol *11*, 1586-1590.

Dentler, W. (2005). Intraflagellar transport (IFT) during assembly and disassembly of *Chlamydomonas* flagella. J Cell Biol *170*, 649-659.

Dilbeck, V., Berberof, M., Van Cauwenberge, A., Alexandre, H., and Pays, E. (1999). Characterization of a coiled coil protein present in the basal body of *Trypanosoma brucei*. J Cell Sci *112*, 4687-4694.

Durand-Dubief, M., Kohl, L., and Bastin, P. (2003). Efficiency and specificity of RNA interference generated by intra- and intermolecular double stranded RNA in *Trypanosoma brucei*. Mol Biochem Parasitol *129*, 11-21.

Efimenko, E., Blacque, O.E., Ou, G., Haycraft, C.J., Yoder, B.K., Scholey, J.M., Leroux, M.R., and Swoboda, P. (2006). *Caenorhabditis elegans* DYF-2, an orthologue of human WDR19, is a component of the intraflagellar transport machinery in sensory cilia. Mol Biol Cell *17*, 4801-4811.

Escalier, D. (2003). New insights into the assembly of the periaxonemal structures in mammalian spermatozoa. Biol Reprod *69*, 373-378.

Estevez, A.M., Kempf, T., and Clayton, C. (2001). The exosome of *Trypanosoma brucei*. Embo J *20*, 3831-3839.

Follit, J.A., Tuft, R.A., Fogarty, K.E., and Pazour, G.J. (2006). The intraflagellar transport protein IFT20 is associated with the Golgi complex and is required for cilia assembly. Mol Biol Cell *17*, 3781-3792.

Grassé, P.P. (1961). La reproduction par induction du blepharoplaste et du flagelle de *Trypanosoma equiperdum*. C. R. Acad. Sci *252*, 3917-3921.

Han, Y.G., Kwok, B.H., and Kernan, M.J. (2003). Intraflagellar transport is required in *Drosophila* to differentiate sensory cilia but not sperm. Curr Biol *13*, 1679-1686.

He, C.Y., Pypaert, M., and Warren, G. (2005). Golgi duplication in *Trypanosoma brucei* requires Centrin2. Science *310*, 1196-1198.

Hou, Y., Qin, H., Follit, J.A., Pazour, G.J., Rosenbaum, J.L., and Witman, G.B. (2007). Functional analysis of an individual IFT protein: IFT46 is required for transport of outer dynein arms into flagella. J Cell Biol *176*, 653-665.

Huangfu, D., Liu, A., Rakeman, A.S., Murcia, N.S., Niswander, L., and Anderson, K.V. (2003). Hedgehog signalling in the mouse requires intraflagellar transport proteins. Nature *426*, 83-87.

Kohl, L., and Bastin, P. (2005). The Flagellum of Trypanosomes. Int Rev Cytol *244*, 227-285.

Kohl, L., Robinson, D., and Bastin, P. (2003). Novel roles for the flagellum in cell morphogenesis and cytokinesis of trypanosomes. Embo J *22*, 5336-5346.

Kohl, L., Sherwin, T., and Gull, K. (1999). Assembly of the paraflagellar rod and the flagellum attachment zone complex during the *Trypanosoma brucei* cell cycle. J Eukaryot Microbiol *46*, 105-109.

Kozminski, K.G., Beech, P.L., and Rosenbaum, J.L. (1995). The *Chlamydomonas* kinesin-like protein FLA10 is involved in motility associated with the flagellar membrane. J Cell Biol *131*, 1517-1527.

Kozminski, K.G., Johnson, K.A., Forscher, P., and Rosenbaum, J.L. (1993). A motility in the eukaryotic flagellum unrelated to flagellar beating. Proc Natl Acad Sci U S A *90*, 5519-5523.

Marshall, W.F., Qin, H., Rodrigo Brenni, M., and Rosenbaum, J.L. (2005). Flagellar length control system: testing a simple model based on intraflagellar transport and turnover. Mol Biol Cell *16*, 270-278.

Marshall, W.F., and Rosenbaum, J.L. (2001). Intraflagellar transport balances continuous turnover of outer doublet microtubules: implications for flagellar length control. J Cell Biol *155*, 405-414.

Moreira-Leite, F.F., Sherwin, T., Kohl, L., and Gull, K. (2001). A trypanosome structure involved in transmitting cytoplasmic information during cell division. Science *294*, 610-612.

Murayama, T., Toh, Y., Ohshima, Y., and Koga, M. (2005). The dyf-3 gene encodes a novel protein required for sensory cilium formation in *Caenorhabditis elegans*. J Mol Biol *346*, 677-687.

Nachury, M.V. et al. (2007). A Core Complex of BBS Proteins Cooperates with the GTPase Rab8 to Promote Ciliary Membrane Biogenesis. Cell *129*, 1201-1213.

Nonaka, S., Tanaka, Y., Okada, Y., Takeda, S., Harada, A., Kanai, Y., Kido, M., and Hirokawa, N. (1998). Randomization of left-right asymmetry due to loss of nodal cilia generating leftward flow of extraembryonic fluid in mice lacking KIF3B motor protein. Cell *95*, 829-837.

Orozco, J.T., Wedaman, K.P., Signor, D., Brown, H., Rose, L., and Scholey, J.M. (1999). Movement of motor and cargo along cilia. Nature *398*, 674.

Ou, G., Koga, M., Blacque, O.E., Murayama, T., Ohshima, Y., Schafer, J.C., Li, C., Yoder, B.K., Leroux, M.R., and Scholey, J.M. (2007). Sensory Ciliogenesis in *Caenorhabditis elegans*: Assignment of IFT components into Distinct Modules Based on Transport and Phenotypic Profiles. Mol Biol Cell. *18*, 1564-1559.

Pazour, G.J., Agrin, N., Leszyk, J., and Witman, G.B. (2005). Proteomic analysis of a eukaryotic cilium. J Cell Biol *170*, 103-113.

Pazour, G.J., Dickert, B.L., and Witman, G.B. (1999). The DHC1b (DHC2) isoform of cytoplasmic dynein is required for flagellar assembly. J Cell Biol *144*, 473-481.

Pedersen, L.B., Geimer, S., and Rosenbaum, J.L. (2006). Dissecting the molecular mechanisms of intraflagellar transport in chlamydomonas. Curr Biol *16*, 450-459.

Pedersen, L.B., Miller, M.S., Geimer, S., Leitch, J.M., Rosenbaum, J.L., and Cole, D.G. (2005). *Chlamydomonas* IFT172 is encoded by FLA11, interacts with CrEB1, and regulates IFT at the flagellar tip. Curr Biol *15*, 262-266.

Piperno, G., and Mead, K. (1997). Transport of a novel complex in the cytoplasmic matrix of Chlamydomonas flagella. Proc Natl Acad Sci U S A *94*, 4457-4462.

Porter, M.E., Bower, R., Knott, J.A., Byrd, P., and Dentler, W. (1999). Cytoplasmic dynein heavy chain 1b is required for flagellar assembly in *Chlamydomonas*. Mol Biol Cell *10*, 693-712.

Pradel, L.C., Bonhivers, M., Landrein, N., and Robinson, D.R. (2006). NIMA-related kinase TbNRKC is involved in basal body separation in *Trypanosoma brucei*. J Cell Sci *119*, 1852-1863.

Qin, H., Diener, D.R., Geimer, S., Cole, D.G., and Rosenbaum, J.L. (2004). Intraflagellar transport (IFT) cargo: IFT transports flagellar precursors to the tip and turnover products to the cell body. J Cell Biol *164*, 255-266.

Ralston, K.S., Lerner, A.G., Diener, D.R., and Hill, K.L. (2006). Flagellar motility contributes to cytokinesis in *Trypanosoma brucei* and is modulated by an evolutionarily conserved dynein regulatory system. Eukaryot Cell *5*, 696-711.

Redmond, S., Vadivelu, J., and Field, M.C. (2003). RNAit: an automated web-based tool for the selection of RNAi targets in *Trypanosoma brucei*. Mol Biochem Parasitol *128*, 115-118.

Rosenbaum, J.L., and Witman, G.B. (2002). Intraflagellar transport. Nat Rev Mol Cell Biol *3*, 813-825.

Sanders, M.A., and Salisbury, J.L. (1994). Centrin plays an essential role in microtubule severing during flagellar excision in *Chlamydomonas reinhardtii*. J Cell Biol *124*, 795-805.

Sarpal, R., Todi, S.V., Sivan-Loukianova, E., Shirolikar, S., Subramanian, N., Raff, E.C., Erickson, J.W., Ray, K., and Eberl, D.F. (2003). *Drosophila* KAP interacts with the kinesin II motor subunit KLP64D to assemble chordotonal sensory cilia, but not sperm tails. Curr Biol *13*, 1687-1696.

Selvapandiyan, A., Kumar, P., Morris, J.C., Salisbury, J.L., Wang, C.C., and Nakhasi, H.L. (2007). Centrin1 Is Required for Organelle Segregation and Cytokinesis in *Trypanosoma brucei*. Mol Biol Cell *18,* 3290-3301.

Sherwin, T., and Gull, K. (1989). The cell division cycle of *Trypanosoma brucei brucei*: timing of event markers and cytoskeletal modulations. Philos Trans R Soc Lond B Biol Sci *323*, 573-588.

Signor, D., Wedaman, K.P., Orozco, J.T., Dwyer, N.D., Bargmann, C.I., Rose, L.S., and Scholey, J.M. (1999). Role of a class DHC1b dynein in retrograde transport of IFT motors and IFT raft particles along cilia, but not dendrites, in chemosensory neurons of living *Caenorhabditis elegans*. J Cell Biol *147*, 519-530.

Smith, D.B., and Johnson, K.S. (1988). Single-step purification of polypeptides expressed in *Escherichia coli* as fusions with glutathione S-transferase. Gene *67*, 31-40.

Snow, J.J., Ou, G., Gunnarson, A.L., Walker, M.R., Zhou, H.M., Brust-Mascher, I., and Scholey, J.M. (2004). Two anterograde intraflagellar transport motors cooperate to build sensory cilia on *C. elegans* neurons. Nat Cell Biol *6*, 1109-1113.

Starich, T.A., Herman, R.K., Kari, C.K., Yeh, W.H., Schackwitz, W.S., Schuyler, M.W., Collet, J., Thomas, J.H., and Riddle, D.L. (1995). Mutations affecting the chemosensory neurons of *Caenorhabditis elegans*. Genetics *139*, 171-188.

Wang, Z., Morris, J.C., Drew, M.E., and Englund, P.T. (2000). Inhibition of *Trypanosoma brucei* gene expression by RNA interference using an integratable vector with opposing T7 promoters. J Biol Chem *275*, 40174-40179.

Wirtz, E., and Clayton, C. (1995). Inducible gene expression in trypanosomes mediated by a prokaryotic repressor. Science *268*, 1179-1183.

Wirtz, E., Leal, S., Ochatt, C., and Cross, G.A. (1999). A tightly regulated inducible expression system for conditional gene knock-outs and dominant-negative genetics in *Trypanosoma brucei*. Mol Biochem Parasitol *99*, 89-101.

Figure legends

Figure 1. IFT and PIFT proteins investigated in this study. Top, diagram (to scale) illustrating the various IFT proteins from complex A and B and PIFT with their specific domains. Bottom, list of IFT proteins and name of their orthologues in *C. reinhardtii*, in *C. elegans* and in *D. melanogaster*. The numbers between parentheses show the percentage of identity between the trypanosome and the indicated orthologous proteins. Most IFT proteins are found in the membrane + matrix fraction of *Chlamydomonas* proteome. MM/Axo: the number of peptides corresponding to each protein found in the membrane + matrix (MM) or the axoneme (Axo) fractions. Data are from the proteomic analysis of the *C. reinhardtii* flagellum (Pazour *et al.*, 2005).

Figure 2. Localisation of IFT proteins in trypanosome flagella. A. Wild-type cells have been fixed in methanol for 5 minutes and stained with a 1:200 dilution of the anti-IFT172 antiserum (green). B. Cells expressing IFT20 fused to a protein A tag stained with the anti-protein A antibody (green) after methanol fixation. C. Direct observation of GFP (green) after methanol fixation of GFP::IFT52 expressing cells. D-F. Cells from the same populations as shown in A-C but that were detergent-extracted to remove the membrane prior to PFA (D,E) or methanol (F) fixation. Only the basal body signal and sometimes the proximal part of the flagellum remain positive. All samples were counterstained with DAPI (blue) to visualise nuclear and kinetoplast DNA. Bar is 5 µm.

Figure 3. GFP::IFT52 is found at the flagellum and the basal body and displays IFT in old and new flagella. A-D. GFP::IFT52 expressing cells were fixed in methanol and stained with different antibody markers of the basal body: MAb22 (A), anti-TBBC (B), 20H5 (anti-

centrins, C) and an antibody raised against the *L. donovani* centrin 1 (D). Direct GFP fluorescence is shown in green, the other antibodies are shown in red and DAPI in blue. Insets show 2.5-fold magnification of the indicated basal body regions. E. Still images of Video S1. The first panel shows a phase contrast image of the cell and the others show a succession of fluorescent images with the elapsed time indicated in seconds. The arrow points at a moving IFT particle. Bar is 5 µm.

Figure 4. IFT particles in flagella of trypanosomes. A-C. Cross sections through the flagella of wild-type (WT) trypanosomes (A-B) or *PF16*^{RNAi} (C) cells induced for 3 days. The presence of the PFR attached to the axoneme allows for unambiguous identification of individual doublets, shown by white numbers. IFT-like particles are indicated by black arrows. D. Position of IFT-like particles relative to axoneme doublets on cross-sections of wild-type (WT), *PF16*^{RNAi} or *PF20*^{RNAi} induced cells for 3 days (n= 42, 81 and 21, respectively). E. Longitudinal section through an IFT-like particle. Note the closer positioning of the flagellar membrane at the particle position. F. Cross-section through both the old (bottom) and the new (top) flagella from a wild-type trypanosome revealing the presence of IFT-like particles in the old flagellum. G. Cross-section through the transition zone showing the 9+0 arrangement but without IFT-like particles. H,I. Cross-sections of flagella of wild-type (WT) trypanosomes close to the top of the flagellar pocket. Central pair and dynein arms are visible but the PFR is not yet present. Abundant particular material can be recognised. J,K. Cross-section through flagella of wild-type or *PF20*^{RNAi} cells induced for 3 days after detergent removal of the membrane. IFT particles are less abundant in detergent-treated samples but can sometimes be recognised (arrow on K). L. Abundance of IFT particles in cross-sections of flagella from whole cells or detergent-extracted cytoskeletons of wild-type (n= 42 and 41, respectively), *PF16*^{RNAi} (n= 82 and 73, respectively) or *PF20*^{RNAi}

(n= 21 and 74, respectively) cells induced for 3 days.

Figure 5. RNAi silencing of *IFT* and *PIFT* genes inhibits new flagellum formation and results in growth arrest. Cell lines were grouped as mutants of genes encoding proteins of complex A (A,D,G), B (B,E,H) or PIFT (C,F,I). A-C. Fields of cells from the indicated cell lines that had been induced for 3 days, stained with the anti-PFR2 L8C4 antibody (green) and with DAPI (blue). A mixture of non-flagellated and flagellated cells was present in all situations. D-F. Proportion of flagellated cells left in the culture of the indicated RNAi mutants during the course of induction of RNAi silencing. G-I. Growth curves of induced (plain lines) and non-induced (discontinuous lines) cells from the indicated RNAi mutants.

Figure 6. IFT proteins from complex A and B are required for flagellum formation but differ in function. A,B. Fields of *IFT88*^{RNAi} (A) or *IFT140*^{RNAi} (B) cells induced for 3 days stained with the anti-IFT172 antiserum (green) and with the MAb25 axoneme marker (red). DNA was stained with DAPI (blue). Cells with a normal-length flagellum (arrows), with a short flagellum (arrowhead) or without visible flagellum (stars) are indicated. C,D. *IFT88*^{RNAi} induced cells have a tiny or no flagellum. E,F. *IFT140*^{RNAi} induced cells exhibit short and dilated flagella accumulating a large amount of IFT172 protein. C, E. Cells induced for 3 days and stained with the anti-IFT172 antiserum (green) and with MAb25 (red). DNA was stained with DAPI (blue). D,F. Scanning electron micrographs. Inset shows a 2-fold magnification of the indicated area. G. Quantification of the number of cells exhibiting accumulation of IFT172 as bright spots during the course of RNAi silencing in the indicated cell lines. H. *IFT140*^{RNAi} cell induced for 3 days with a short new flagellum and an old flagellum. Only the new flagellum is too short, dilated and accumulates IFT172 protein. Cells were stained with the anti-IFT172 antiserum (green) and with DAPI (blue). Bar is 5 µm.

Figure 7. Formation of the new flagellum in wild type cells and its inhibition in *IFT*^{RNAi} cell lines. Sections through the flagellar pocket of wild-type (WT, A-E) or *IFT172*^{RNAi} cells induced for 48 h (F) or of *IFT88*^{RNAi} (G), *DHC1b*^{RNAi} (H,I) induced for 72 hours. Notice the large amount of material only in very short flagella of wild-type cells (B,C). The arrow on panel B indicates the new flagellum. The new flagellum grows in the same flagellar pocket as the old one (B, D) and elongates until two separate flagellar pockets are recognised (E). Bald basal bodies (F, G) were frequent in sections of induced *IFT172*^{RNAi} and *IFT88*^{RNAi} mutants whereas short flagella and accumulation of IFT material was common in *DHC1b*^{RNAi} induced cells (H, I). Bars are 500 nm except where indicated.

Figure 8. PIFT are involved in anterograde or retrograde transport. *PIFTB2*^{RNAi} (A) and *PIFTC3*^{RNAi} (B) induced for 3 days and *PIFTD4*^{RNAi} (C) induced for 5 days were stained with the anti-IFT172 antiserum. D. Proportion of short cells displaying no, weak or bright signal with the anti-IFT172 antiserum ($n \geq 100$). Bar is 5 µm.

Figure 9. Inhibition of IFT does not prevent flagellum membrane elongation. A. After RNA silencing of *IFT* and *PIFT* genes, five categories of cells were defined, illustrated here in *PIFTF6*^{RNAi} cells induced for 4 days: cells (a) with no recognisable structures (grey code); (b) without flagella but with a surface "depression" (light blue); (c) with tight or (d) disperse rows of vesicles that emerge from a "depression" without recognisable flagellar structure (dark blue); (e) short flagella alone (orange) and (f) short flagella with a 'flagellar sleeve' as described by Davidge *et al*. (2006)(red). Yellow arrowheads and arrows indicate cell depressions and short flagella, respectively. B. Frequency of each cell types in the indicated cell lines (cells with flagella longer than 2 µm were not included). C. Section through the flagellar sleeve of *IFT172*^{RNAi} cells induced for 2 days.

Table 1. Effects of RNAi silencing of IFT genes on axonemal microtubule elongation

Cell line	BB with axoneme microtubules	BB with interrupted microtubules	Bald BB	n
Wild-type	89 %	0 %	11 %	46
IFT88^{RNAi}	14 %	7 %	79 %	14
DHC1b^{RNAi}	28 %	15 %	56 %	32

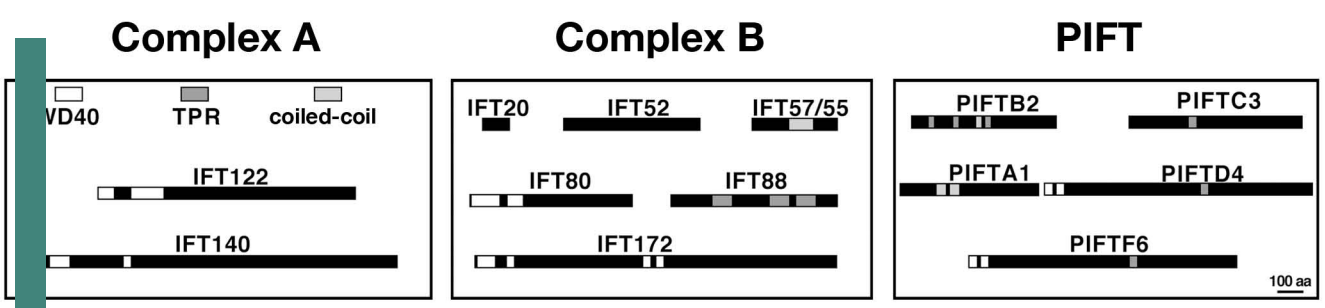

Name	*T. brucei*	*C. reinhardtii*	*C. elegans*	*D. melanogaster*	MM/Axo
Complex A					
IFT122	Tb10.70.1660	IFT122 (36)	DAF10 (31)	OSEG1 (31)	0/0
IFT140	Tb10.61.2260	IFT140 (32)	CHE11 (27)	OSEG3 (29)	17/0
Complex B					
IFT20	Tb927.6.3290	IFT20 (36)	Y110A7A.20 (23)	CG30441 (31)	5/0
IFT52	Tb10.61.1590	IFT52 (37)	OSM6 (29)	CG9595 (25)	5/0
IFT57/55	Tb10.26.0670	IFT57/55 (29)	CHE13 (30)	CG8853 (26)	7/0
IFT80	Tb10.61.1560	IFT80 (43)	CHE2 (29)	OSEG5 (27)	6/0
IFT88	Tb11.55.0006	IFT88 (39)	OSM5 (32)	NOMPB (26)	14/0
IFT172	Tb10.70.6920	IFT172 (41)	OSM1 (30)	OSEG2 (33)	46/0
Putatively involved in IFT (PIFT)					
PIFTA1	Tb927.3.1110	C_158863 (31)	DYF3 (21)	CG17599 (23)	5/0
PIFTB2	Tb927.3.5490	FAP259 (55)	DYF1 (42)	CG5142 (40)	2/0
PIFTC3	Tb927.3.3000	C_154165 (51)	DYF13 (33)	CG4525 (41)	0/0
PIFTD4	Tb927.5.3030	FAP118 (37)	IFTA1 (26)	OSEG4 (35)	9/0
PIFTF6	Tb11.03.0880	FAP66 (30)	DYF2 (27)	OSEG6 (27)	22/0
Motor					
DHC1b	Tb11.02.0030	DHC1b (34)	CHE3 (27)	CG15148 (27)	85/3

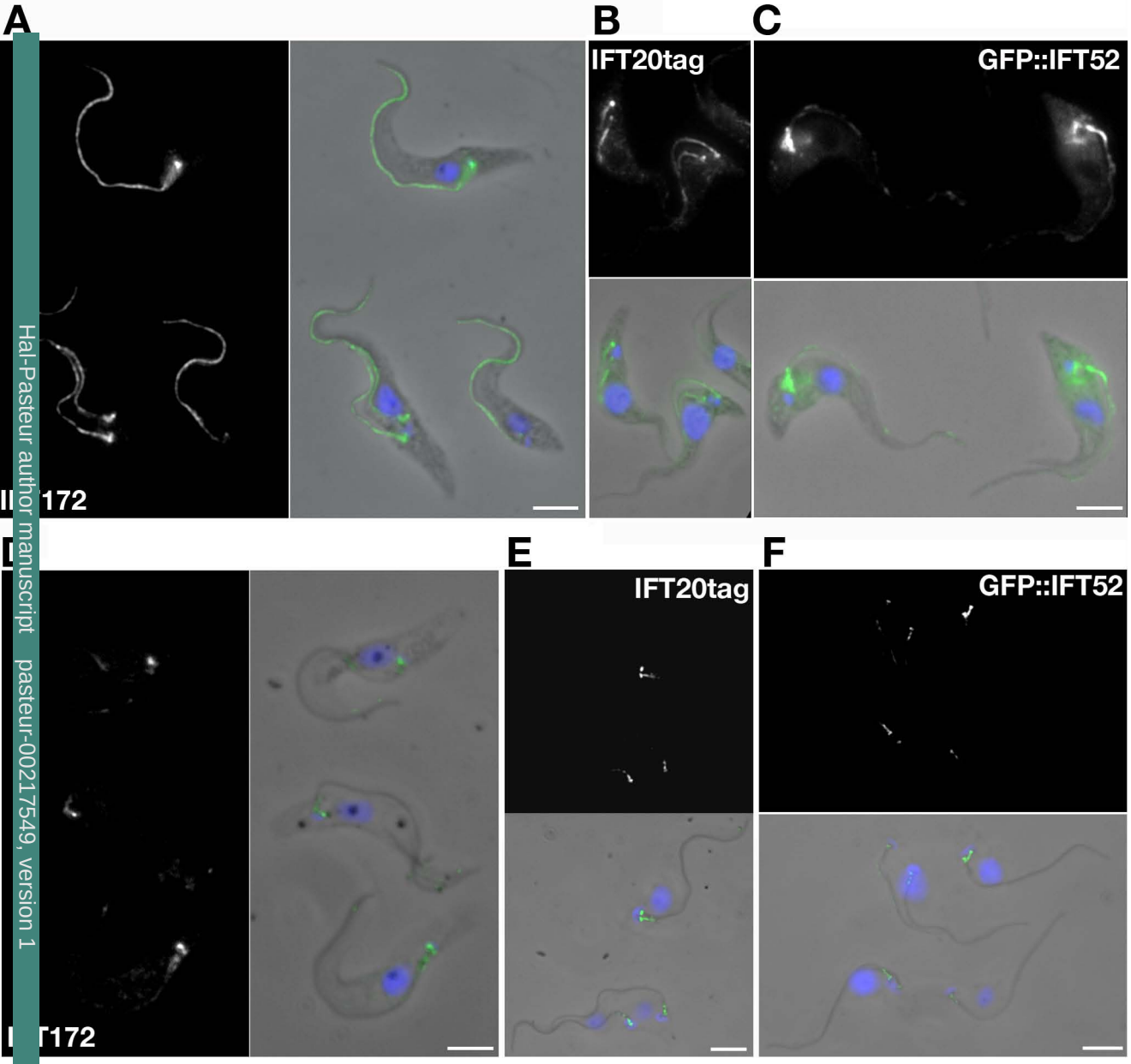

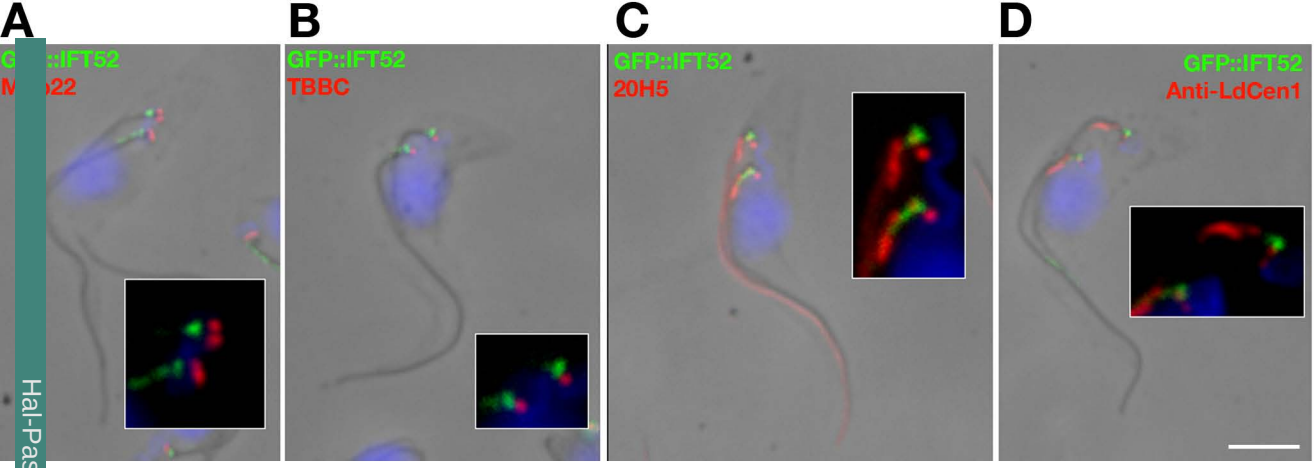

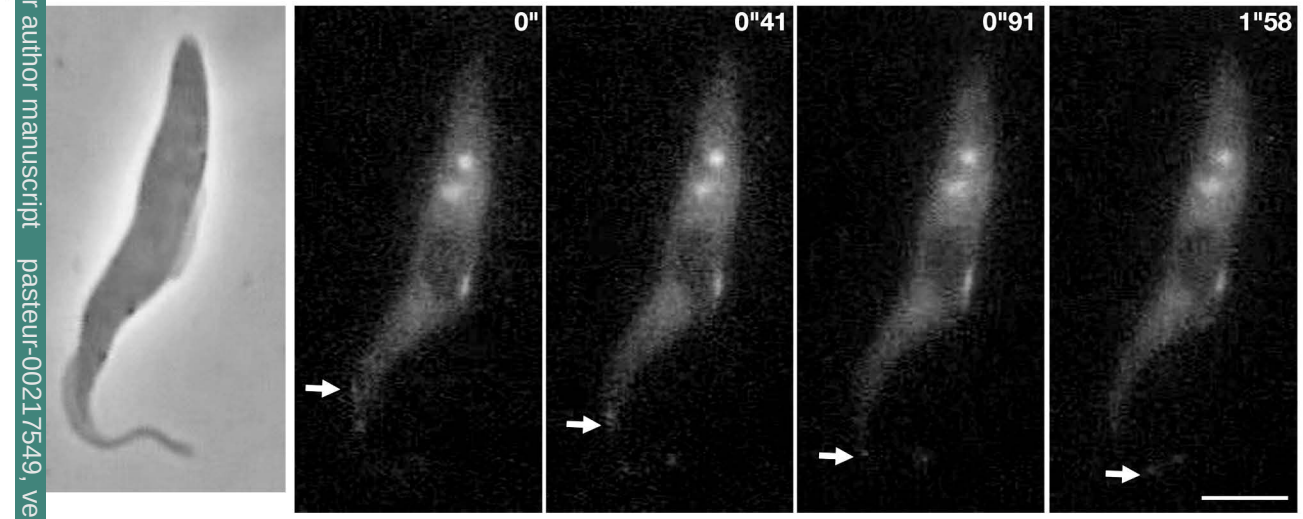

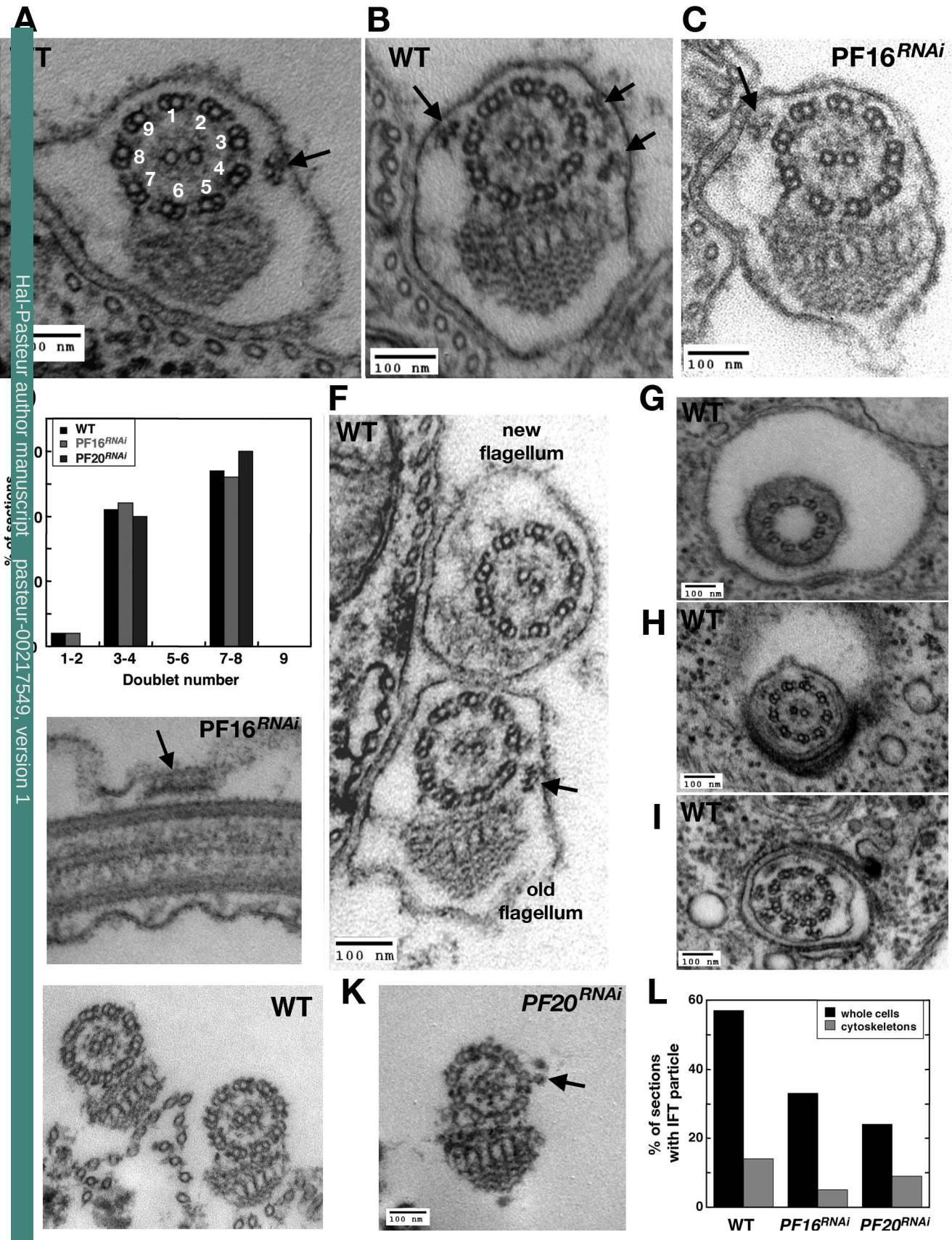

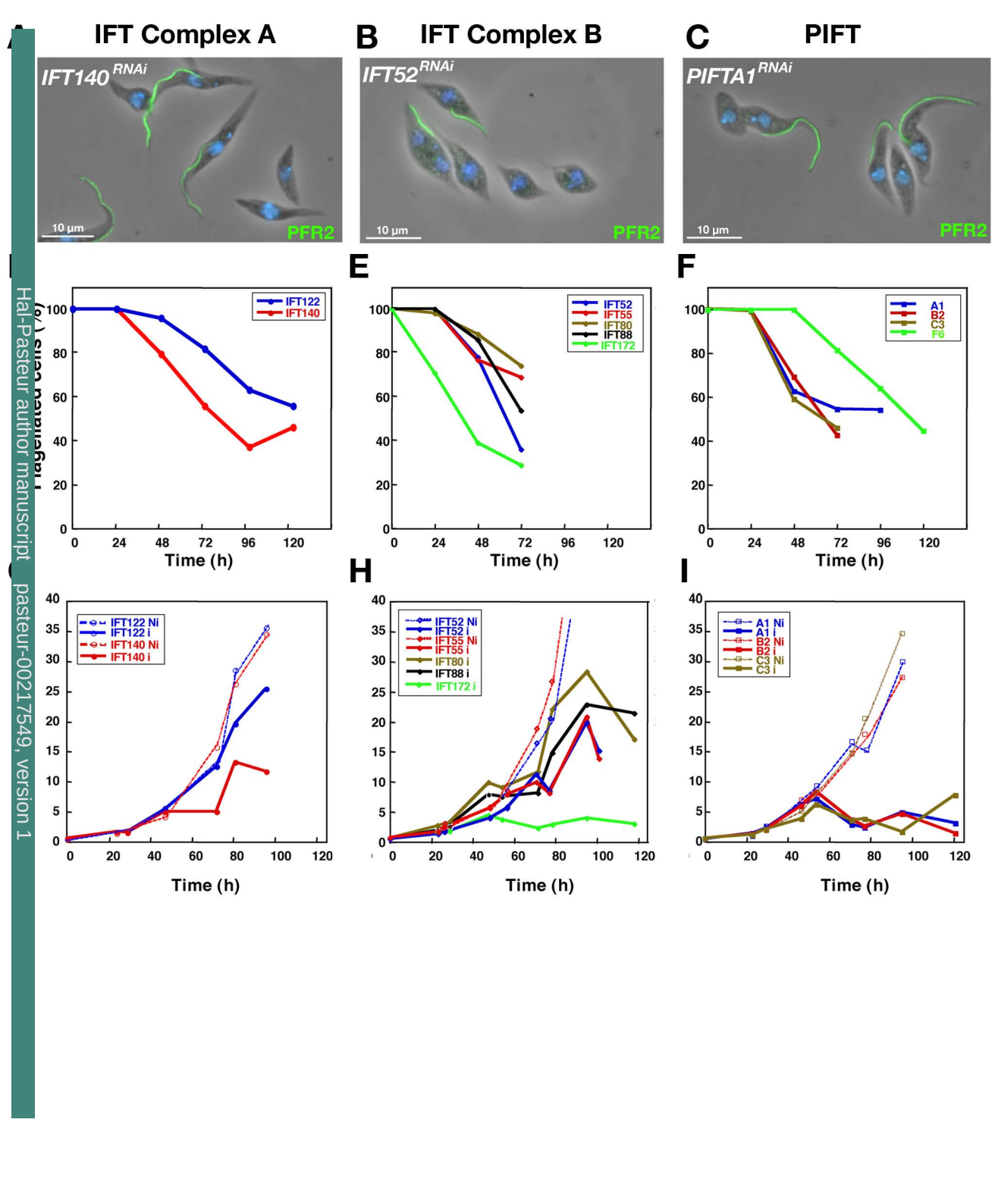

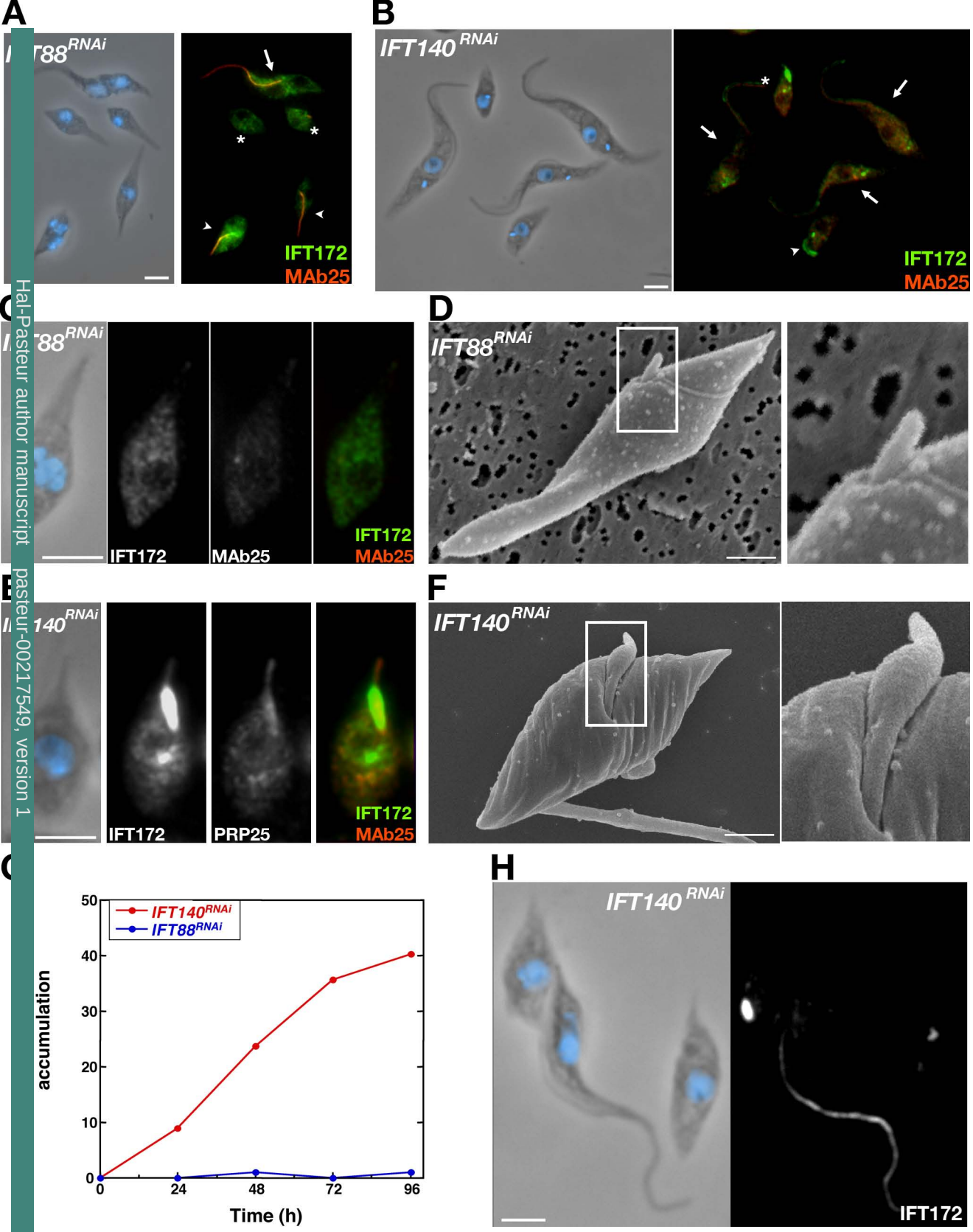

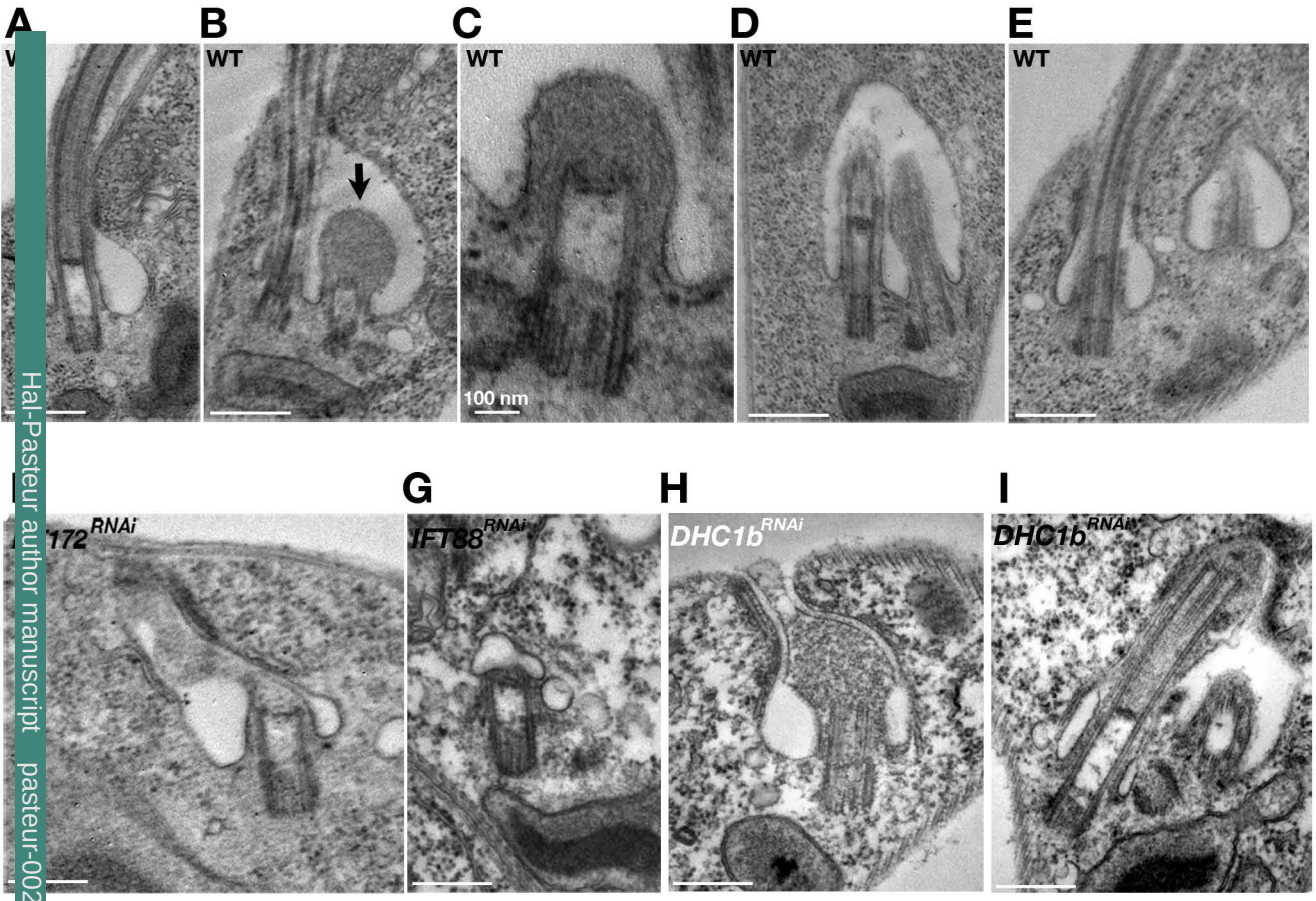

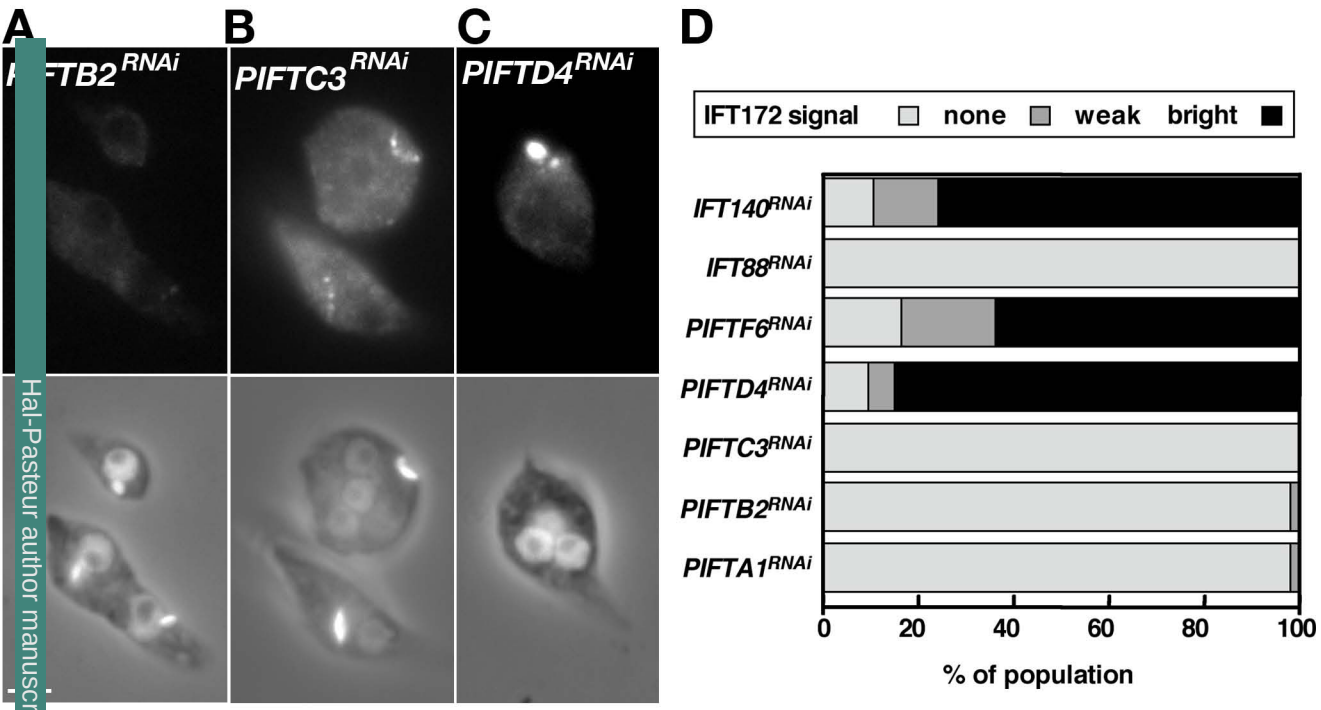

A

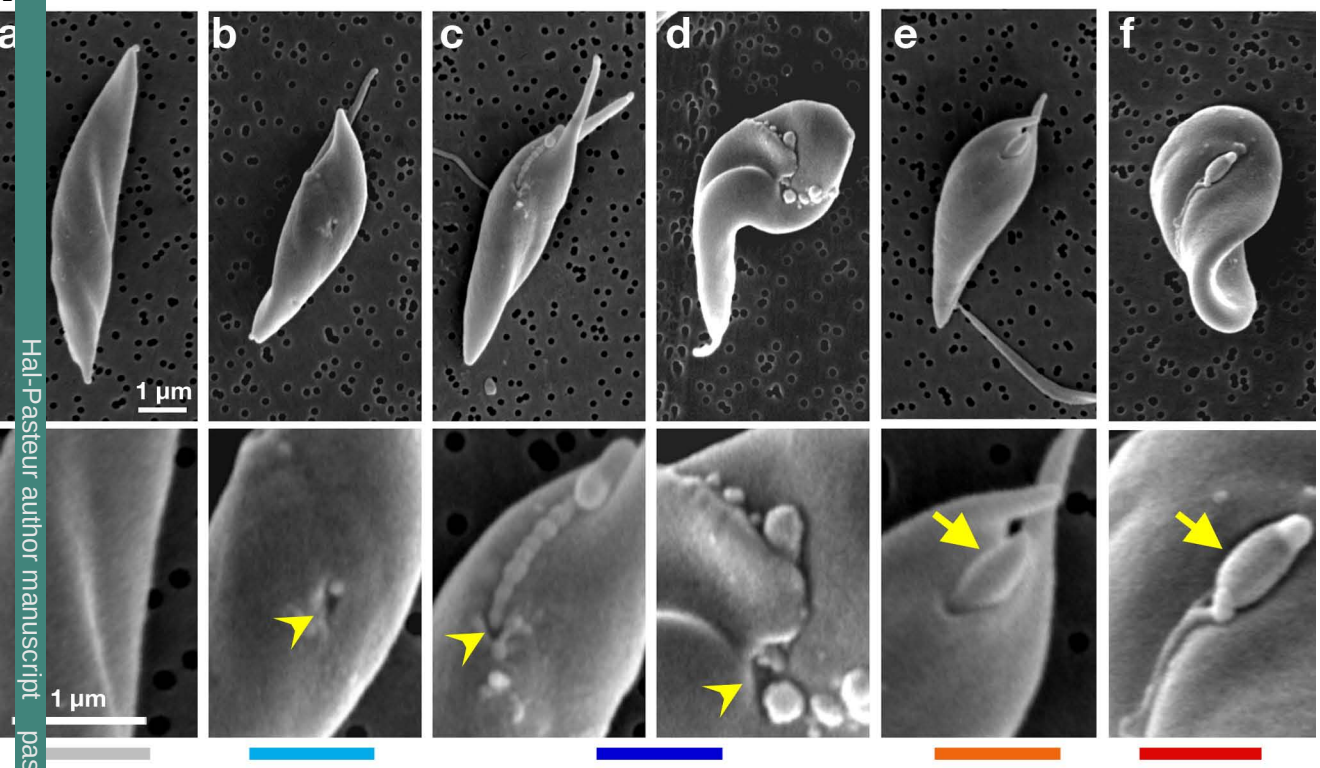

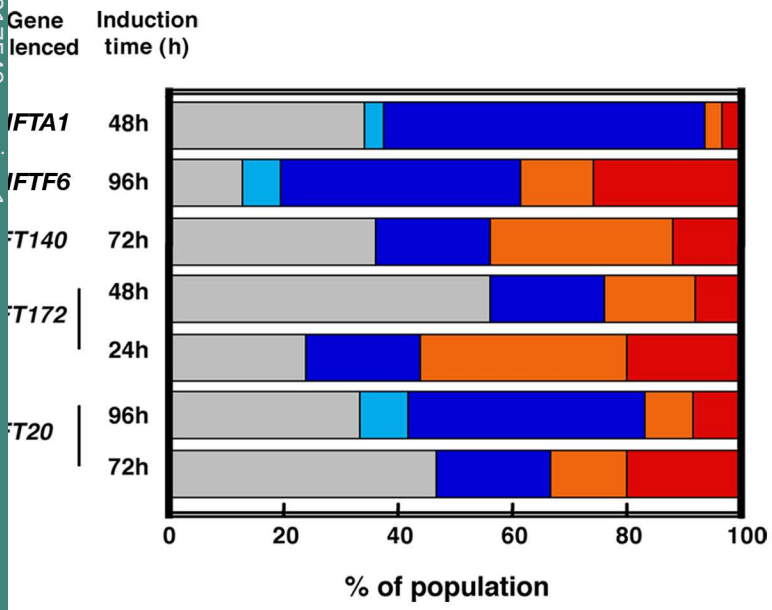

C